Quantitative compositional analysis of Martian mafic regions using the MEx/OMEGA reflectance data: 2. Petrological implications

François Poulet, N. Mangold, B. Platevoet, J.-M. Bardintzeff, V. Sautter, J.F. Mustard, J.-P. Bibring, P. Pinet, Y. Langevin, B. Gondet, et al.

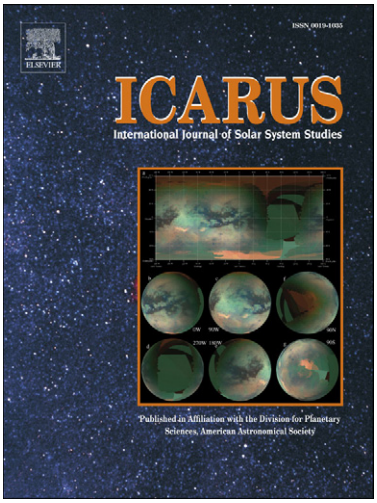

Quantitative compositional analysis of Martian mafic regions using the MEx/OMEGA reflectance data: 2. Petrological implications

F. Poulet, N. Mangold, B. Platevoet, J.-M. Bardintzeff, V. Sautter, J.F. Mustard, J.-P. Bibring, P. Pinet, Y. Langevin, B. Gondet, A. Aléon-Toppani

PII: S0019-1035(09)00014-1
DOI: 10.1016/j.icarus.2008.12.042
Reference: YICAR 8881

To appear in: *Icarus*

Received date: 23 July 2008
Revised date: 24 November 2008
Accepted date: 22 December 2008

Please cite this article as: F. Poulet, N. Mangold, B. Platevoet, J.-M. Bardintzeff, V. Sautter, J.F. Mustard, J.-P. Bibring, P. Pinet, Y. Langevin, B. Gondet, A. Aléon-Toppani, Quantitative compositional analysis of Martian mafic regions using the MEx/OMEGA reflectance data: 2. Petrological implications, *Icarus* (2009), doi: 10.1016/j.icarus.2008.12.042

Quantitative compositional analysis of Martian mafic regions using the MEx/OMEGA reflectance data: 2. Petrological implications

F. Poulet[1], N. Mangold[2], B. Platevoet[3], J.-M. Bardintzeff[3,7], V. Sautter[4], J. F. Mustard[5], J.-P. Bibring[1], P. Pinet[6], Y. Langevin[1], B. Gondet[1], A. Aléon-Toppani[1]

[1]Institut d'Astrophysique Spatiale, Université Paris-Sud, Orsay Cedex, 91405, France

[2]Lab. de Planétologie et Géodynamique, UMR6112, CNRS et Université de Nantes 2 rue de la Houssinière, BP 92208, 44322 Nantes cedex 3 France

[3]IDES, Bât. 509, Université Paris-Sud, 91405 Orsay Cedex, France

[4]Laboratoire Minéralogie-Pétrologie, Museum National d'Histoire Naturelle, Paris, France

[5]Department of Geological Sciences, Brown University, Providence, USA

[6]Observatoire Midi-Pyrénées, 31400 Toulouse, France

[7]IUFM, Université de Cergy-Pontoise, RP 815, 78008 Versailles, France

Proposed running head: Martian petrology

Send correspondence to:

François Poulet

Institut d'Astrophysique Spatiale

Bâtiment 121, Université Paris-Sud

91405 Orsay Cedex

France

Phone: +33169858582

Email: francois.poulet@ias.u-psud.fr

Abstract

The primary objectives of this paper are to determine the modal mineralogy of selected low albedo terrains of different ages ranging from Noachian to Amazonian exposed on the surface of Mars. This analysis is conducted using the spectral modelling of the Observatoire pour la Minéralogie, l'Eau, les Glaces, et l'Activité (OMEGA) reflectance data. Results from this work are consistent with the major results of previous spectroscopic studies: plagioclase (40-60% in volume) and high calcium pyroxene (20-40%, HCP) are the dominant minerals of the most regions. Low calcium pyroxene (10-15%, LCP) and minor amounts of olivine are also present. The oldest terrains are characterized by the largest amount of LCP and the lowest concentration of plagioclase. These overall compositions are consistent with two-pyroxene basalts. The particle sizes are in the range of a few hundreds of micrometers, which is in good agreement with the thermal inertia of the Martian low albedo regions. In the region around the Nili Fossae, localized concentrations of olivine up to 40% with millimetre particle size similar to picritic basalts observed in situ by the Spirit rover in the Gusev crater are inferred. Chemical compositions are calculated for the first time from OMEGA spectra. They are quite consistent with Gusev rocks and Shergottite compositions but they appear to be significantly SiO_2-poorer than Thermal Emission Spectrometer data.

A decreasing low calcium pyroxene abundance with the decreasing age of the low albedo regions is reported. This may be indicative of decreasing degree of partial melting as thermal flux decreases with time. We propose that the ancient Noachian-aged, LCP-rich terrains could have been formed from H_2O-bearing melts. Then, dry, basaltic volcanism occurred leading to decreasing LCP abundance with time due to decreasing degree of partial melting.

The olivine-bearing material modeled in Nili Fossae resembles the composition of ALH77005 and Chassigny meteorites consistent with prior studies. Implications on the formation of the basaltic Shergottites are discussed.

1. Introduction

The spatial distributions, abundances, and particle sizes of mineral phases on Mars have important petrogenetic implications for the Martian mantle and crust. The Observatoire pour la Minéralogie, l'Eau, les Glaces et l'Activité (OMEGA) instrument aboard the Mars Express spacecraft began collecting visible and near-infrared (0.4-5.1 μm) reflectance data from Mars in 2004 (Bibring et al., 2004). One of the major science objectives of OMEGA is to map the mineralogy of the Martian surface, in order to improve understanding of Martian crust and mantle composition and evolution. The first global analysis of reflectance OMEGA spectra showed that the low albedo regions could generally be grouped into different classes (Mustard et al., 2005; Bibring et al., 2005; Poulet et al., 2007): distinct mafic, rock-forming minerals low-calcium pyroxene (LCP), and high-calcium pyroxene (HCP) are identified in equatorial and southern low albedo regions; the regions exhibiting the strongest LCP signatures are found mainly in the ancient Noachian-aged units; olivine with high iron content and/or large particle size (>100 μm) is only detected in isolated areas, olivine (Mg-rich composition) is detected in extensive regions of the pyroxene-rich zones; extended dark regions in the northern plains exhibit shallow pyroxene absorptions. A companion paper (Poulet et al., 2008; hereinafter referred to as Paper 1) demonstrated that a nonlinear spectral mixing method, based on the Shkuratov radiative transfer theory, could successfully model OMEGA spectra and provide modal mineralogy within the uncertainties of the modeling (vol 5-15% depending on the minerals). On the basis of the applications reached in Paper 1, the objective of this work is to: 1) determine the modal mineralogy of a variety of unaltered mafic-rich regions, which happen to be of low albedo regions using OMEGA data, 2) clarify the mineral distributions previously identified in Poulet et al. (2007), 3) compare the modal and chemical composition with those derived from Thermal Emission Spectrometer (TES) analyses (Bandfield et al., 2000; Christensen et al., 2000a; Christensen et al., 2001; Bandfield,

2002; Hoefen et al., 2003; McSween et al., 2003; Rogers and Christensen, 2007; Koeppen and Hamilton, 2008), 4) identify possible relationship with the diverse compositions of SNCs, 5) evaluate constraints on the chemistry and petrology of the ancient crust, and 6) explore how crustal components identified here might have arisen on Mars.

2. Previous works on crustal composition

The igneous composition of the Martian crust has been examined through SNC meteorites, remotely sensed data, and in situ observations by landers and rovers (e.g., McSween et al., 2003; 2008 and references therein). Meteorites exhibit the greatest petrologic diversity subdivided into basaltic Shergottites (tholeiitic basalts), olivine-phyric Shergottites (basalts containing olivine xenocrysts or phenocrysts), lherzolitic Shergottites (plagioclase-bearing peridotites), Nakhlites (olivine-bearing clinopyroxenites), Chassignites (dunites), and orthopyroxenite ultramafic cumulate (ALH84001) (Lodders, 1998; Dreibus et al., 2000; Folco et al., 2000; Rubin et al., 2000; Barrat et al., 2002; Taylor et al., 2002; Imae et al., 2003).

Visible/near-infrared (VNIR) and thermal infrared (TIR) remote spectroscopic observations have revealed that pyroxenes, plagioclase, and high-silica phase(s) dominate the mineralogy of low albedo terrains (McCord et al., 1978; Pinet and Chevrel, 1990; Bell et al., 1997; Mustard et al., 1997; Christensen et al., 2000a; Bandfield et al., 2000; Bandfield, 2002; Mustard et al., 2005). OMEGA observations identified olivine- and HCP-bearing regions in terrains that span the age range of major geologic units (Mustard et al., 2005; Poulet et al., 2007), while the strongest signals of LCP are focused in the ancient cratered terrain. There have been also a few outcrops of ancient crust identified in thermal emission data that exhibit concentrations of olivine (Hoefen et al., 2003) and LCP above the limits of detection (Hamilton et al., 2003). Several detailed analyses of some low albedo regions have identified local occurrences of unique mineralogy such as olivine-basalts (Hoefen et al., 2003; Hamilton

and Christensen, 2005; Rogers et al., 2005; Mustard et al., 2007; Poulet et al., 2007) and perhaps quartz-rich terrains (e.g., Bandfield et al., 2004).

Volcanic rocks excavated from craters on the floor of Gusev Crater are picritic basalts that share many similarities with olivine-phyric Shergottites (McSween et al., 2006a). Cross comparisons of OMEGA and Opportunity observations demonstrate that the plains of Meridiani are dominated by a basaltic sand cover with a lag concentration of hematitic concretions (Arvidson et al., 2006). However, this sand has an unclear origin and may not representative of the nature of the low albedo regions. Bounce rock, an anomalous 35-cm rock on the sands of Meridiani has a distinctive X-Ray, Mössbauer, and Mini-TES spectrum not seen at the MER landing sites (Squyres et al., 2004a). Specifically, this rock has a spectrum like those of the pigeonite-rich Shergottites (Christensen et al., 2004).

3. Approach

3.1. Overview

The OMEGA spectral range extends from 0.36 to 5.09 μm (Bibring et al., 2004). It is covered by a visible channel (96 wavelengths from 0.36 to 1.07 μm) and two IR channels (C: 128 wavelengths from 0.92 to 2.7 μm; L: 128 wavelengths from 2.53 to 5.09 μm). The pixel size (from 300 m to a few kms) is proportional to the altitude of the spacecraft that has an elliptical orbit. The OMEGA radiance data are corrected for solar irradiance and atmospheric absorptions in the NIR using the standard data reduction schemes, which produces reflectance atmospherically corrected I/F spectra (Langevin et al., 2007). We have used the OMEGA data recorded when the operation mode is nadir and selected OMEGA cubes with low aerosol opacity. By applying classical methods of spectral identification based on spectral parameters to atmospherically corrected I/F reflectance specra, OMEGA has provided consistent identification and spatial distribution of several classes of mafic minerals (Poulet et al., 2007).

The next step in analysis of the OMEGA spectra is to perform a quantitative retrieval of mineral abundances from the modeling of spectra of the well-calibrated C channel. The previous investigations discussed in paper 1 have revealed many of the details of the method used to model and interpret the OMEGA spectra of mafic-rich terrains. Specifically, any OMEGA spectrum may be closely modeled using a nonlinear combination of selected end-member optical properties weighted by the abundance and the particle size of each end-member. The data set and methods have been demonstrated to be consistent and robust, enabling the transition from spectral unit maps to modal mineralogy maps; it also allows a first systematic exploration of the modal mineralogy as determined by the OMEGA instrument. However, modeling based on radiative transfer calculation requires significant computing time, and thus we model specific, representative regions, rather than the entire OMEGA data set.

There is another reason to examine the surface composition of low albedo regions. Rogers and Christensen (2007) recently demonstrated that subtle, but spatially coherent thermal infrared spectral differences exist between certain low albedo regions. Deconvolving these data into modal abundances, they found that Martian dark regions could be classified into four groups based on relative abundances of plagioclase, pyroxene, olivine, and high-silica phase(s) (primary or secondary silicate minerals, glasses or amorphous with Si/O ratios > 0.35), that differ by ~10% or more between groups. Our study will therefore focus partly on the regions previously investigated by TES. The northern low albedo regions, which best illustrate the TES surface type 2, are not considered because the very shallow mafic signatures make difficult the modeling in the NIR spectra. Actually, chemical alteration or oxidation during extrusion producing a coating or varnish of anhydrous ferric phases over a dark basaltic surface best accounts for the VNIR spectral properties of these regions (Poulet et al., 2007). Such a mixture cannot be simulated by our present model, which preferentially applies

to granular- or bedrock- type surface (Poulet and Erard, 2004). Surface type 2 has nevertheless significant concentrations scattered throughout the southern highlands (Bandfield, 2002), and one of these regions (Solis Lacus) is examined.

3.2. Non-linear spectral modeling

We use the radiative transfer model described in paper 1 to fit OMEGA atmospherically corrected spectra of C channels 5 to 112 corresponding to 0.997 and 2.50 μm. The quality of the fit is evaluated by the value of the Residual Mean Squared (RMS). A skeleton library consisting of optical constants of a minimum amount of end-members to account for all major igneous minerals was compiled for use in paper 1: LCP (pigeonite), HCP (diopside), Fe-rich olivine (fayalite), Mg-rich olivine (Fo90), and plagioclase (labradorite) with dark oxide (magnetite) inclusions embedded. Martian dust was added to represent the mobile dusty component identified by its ferric bands detected in the visible part of the spectra. Augite is a possible end-member but not included here. The influence of this mineral was evaluated on the final abundances of HCP end-member and other phases (paper 1). It has been shown that taking this mineral instead of diopside as the HCP end-member decreases the abundance of the HCP end-member by a few percent. Orthopyroxenes such as hypersthene are not considered as end-member because their bands are so strong in comparison to the low calcium clinopyroxenes such as pigeonite (Cloutis and Gaffey, 1991), that none satisfactory fit of the spectra could be obtained with these minerals.

The free parameters are the abundance and the particle size of each mineral, except for the magnetite inclusions, the dust component and the olivine. The dark oxide being inclusions embedded in the matrix, the particle size is not a parameter (Poulet et al., 2002). As discussed in the companion paper, the particle size of the dust component is fixed at 5 μm. Apart from the olivine-rich terrains discussed in section 4.2, the olivine abundance is given assuming

forsterite as end-member and particle size fixed at 100 μm. In addition, a single free parameter is used to adjust the continuum spectral slope so as to account for the contribution of aerosols and/or photometric effects.

3.3. Study areas

3.3.1. Data selection

Maps of the geographic locations discussed in this work are provided in Figures 1 and 2, and the characteristics of the studied regions are detailed in Table 1. The regions are mainly representative of the Noachian and Hesperian low albedo regions of Mars and sample different types of terrains: lavas, cratered terrains, dissected terrains. These regions are sampled by several thousand spectra. Dust-free mafic terrains from Amazonian period are sparse on the surface of Mars. A couple of small areas classified as young terrains are however identified in the Tharsis region (Fig. 1). Small outcrops enriched in LCP are also examined. In addition, the mineralogy of some olivine-bearing terrains (Nili Patera and dunes in Syrtis Major, Nili Fossae) is derived (Fig. 2). The LCP- and olivine-bearing terrains are small, so that the errors on the output parameters may be expected to be larger than for the extended low albedo regions. A more systematic study of LCP- and olivine-bearing terrains will be done in further studies.

For each region, the values for any mineral will refer to an average of the final abundances calculated for all the spectra of the studied region. Using this method, a regionally dominant modal mineralogy should be derived, so that global trends in the distribution of the mineral phases can be better compared. The potential disadvantage is that local-scale enrichments in a single mineral group can be obscured. At the OMEGA pixel spatial sampling, there are variations of the final abundances, which are well correlated with the intensity and the shape of the mafic signatures as well as with geomorphologic characteristics.

Olivine- and LCP-bearing terrains are mainly representative of such local scale variations, and we have selected several of theis for analysis (Tables 1 and 2). As described below, most of the studied regions present relatively homogeneous mafic signatures, as well as relative homogeneous geological characteristics, so that the inferred average mineralogy reflects a homogenous surface composition rather than a mixture of the regional composition with abundant local-scale outcrops that are enriched in a particular mineral group.

Aeolian transport is also likely to influence the distribution of minerals on Mars (Edgett and Christensen, 1991; Rogers and Christensen, 2003). This raises the question of whether the materials in the studied regions are of local origin (derived from bedrock of the underlying unit) or regional origin (derived from bedrock several hundreds of kilometers away), and whether particle sorting does modify the initial composition of this bedrock. If broad-scale transport occurred, it is likely that very homogeneous spectral shapes, representing mixtures of the original compositions, would be detected. Supporting evidence that this transport does not strongly affect the composition surface comes from the existence of distinct, spatially separated surface units of well-crystalline hematite, basalt, olivine, sulfates and clay mineral units (Christensen et al., 2000b; Gendrin et al., 2005; Poulet et al., 2005). This demonstrates that global mixing of sand-sized particles (>100 μm) has not occurred, and that the variations from region to region can be evaluated within the uncertainties of the modeling. Dust storms are also expected to modify the surface composition. However, widespread transient dust deposits are not observed over dark areas in the NIR after the major dust storms (Vincendon et al., 2008). This implies that either dust is not significantly deposited on most dark terrains or dust is rapidly removed by cleaning mechanisms.

For sand-rich regions, we consider that the mean composition of the surface covered by sand represents an average of the composition of the bedrock as usually assumed in TES

studies. However, local sorting of bedrock grains might occur, which can modify the composition along the wind transport direction. Using TES thermal inertia from Putzig et al. (2005) and geomorphology (see next sections), we have sampled many regions that display more or less sand component, in order to avoid a systematic effect of sand transport.

3.3.2. Noachian sites

The region around the Nili Fossae region exhibits very diverse spectral signatures (Poulet et al., 2005; Baratoux et al., 2007; Mustard et al., 2007; Mangold et al., 2007). The area chosen for the modeling is located north of a strongly altered unit, in a part of the bedrock which does not display a massive alteration. Thermal inertia varies from 200 to 500 $J/m^2/K/s^{1/2}$ (hereafter TIU) locally, suggesting a variety of particles from fine sand to coarser grains mixed with bedrock (Kieffer et al., 1977; Presley and Christensen, 1997; Pelkey et al., 2001; Putzig et al., 2005). However, no sand sheets or dunes are visible on Mars Orbiter Camera (MOC) images suggesting that the surface is rough, simulating sand-sized thermal inertia. In contrast, the Nili Fossae olivine rich area is located in a place with extensive dune activity (see Mangold et al., 2007 for location). The age of the olivine-bearing unit is likely Late Noachian and it could correspond to the impact melt of Isidis basin (Mustard et al., 2007). Whatever the interpretation, it is clear that the olivine-bearing material sits on phyllosilicate-bearing terrain mostly, sometimes LCP-bearing, which indicates that the olivine-bearing material formed later (Mustard et al., 2007; Mangold et al., 2007).

Three Noachian-aged, LCP-rich areas were chosen for modeling (Fig. 3). Two of them consist of small highland outcrops of Early to Middle Noachian age. The third one is a hill located inside a canyon south of Coprates Chasma, LCP is found in the basal part of the Valles Marineris walls. From the size of each selected area and its hilly topography, these outcrops are intrepreted to be bedrock and not sand sheets.

The low albedo region located in the Terra Meridiani is studied in detail in Paper 1. It consists of smooth plains commonly covered by sand dunes (Arvidson et al., 2003). Indeed, this terrain is very smooth with thermal inertia between 200 and 400 TIU. This unit has been interpreted as a Noachian unit by Arvidson et al. (2003).

3.3.3. Hesperian sites

Hesperian volcanic provinces that display mafic NIR signatures are common on Mars (Fig. 4). Hesperia Planum is a typical Early Hesperian ridged plain (Greeley and Guest, 1987, Mangold et al., 2000). At MOC scale the surface is typically smooth with local rocky outcrops. The thermal inertia is low to intermediate with 200 to 350 TIU (Putzig et al., 2005). These observations suggest a high degradation of the material into fine sand. Given the size of the plain, it is very likely that the sand is derived from regional accumulation of the plains material.

The Protei Planum terrain is located in a Early Hesperian plain (Scott and Tanaka, 1986). The thermal inertia locally reaching 770 TIU suggests large exposure of rocks to the south. Intermediate values of about 300 to 400 TIU are found in the plains suggesting a contribution of sand there, but coarser than in Hesperia Planum.

The plain chosen in Terra Tyrrhena is located south of a highland terrain with two large craters (> 40 km in diameter). It displays a smooth surface at low resolution with wrinkle ridges typical of ridged plains. We derive an age from crater counts over an area of 13,000 km^2. We find the numbers of craters >5 km as N(5)=224+/-127 craters/10^6 km^2, and >2 km as N(2)=972+/-261 craters/10^6 km^2. Within the uncertainty, these counts lead to an age at the very end of the Noachian and beginning of the Hesperian. Thermal Emission Imaging System (THEMIS) images show a relatively rocky terrain but intermediate TES thermal inertias (250 to 360 TIU) also suggest a sand mantling. Nevertheless, the texture visible over two MOC images at the edge of the plain is very rough, and we lack data that would confirm

the presence of sand in the center of the plain. We have focussed our analysis on the ridged plain that appears to be homogeneous in age and geologic style, and which displays locally rocky outcrops.

Mare Sirenum is a region composed of a few ridged plains interupted by local Noachian highlands. We limit our data processing to the part of ridged plains which are dated of the Early Hesperian epoch (Scott and Tanaka, 1986). Thermal inertia varies from 150 to 400 TIU there, with most of the plain studied above 250 TIU suggesting a mixture of sand and rocky outcrops.

Syrtis Major Planum is the most typical region of Mars in terms of mafic mineralogy (e.g., Mustard et al., 1993; Hiesinger and Head, 2004). The area selected is located southwest of Nili and Meroe Paterae (Table 1). This province was mapped as a typical Early Hesperian plains (Hiesinger and Head, 2004), despite a slightly younger age (end of Early Hesperian and beginning of Late Hesperian) as given by other studies (Greeley and Guest, 1987; Mangold et al., 2000). The area of the Paterae is considered as Late Hesperian. MOC images show that the selected area, located at the small west of the province, is covered extensively by sand sheets and dark material of particles likely finer than sand (Poulet et al., 2003). The thermal inertia varies from 140 to 320 TIU, which confirms this interpretation. Because the wind blows from NE to SW in Syrtis Major, small particles there are likely due to an accumulation at a regional scale. This leads to the problem of sand sorting, which could modify slightly the initial composition, but enables us to extract a homogeneous composition on a large terrain.

The selected zone of Solis Lacus is located south of the large Coprates-Solis Planum lava plain in a section displaying well exposed lava flows as seen from the THEMIS day time image. Relative high TES thermal inertia (from 330 to 500 TIU) suggests coarser or more indurated material than in Hesperia Planum and many rocky outcrops of lava flows are visible in MOC images. Taken together, these data show the presence of volcanic material exposure

with little sand accumulation. The terrain is homogeneous in age, established to be Late Hesperian (Scott and Tanaka, 1986), as well as in geology enabling us to extract the average composition without problems regarding sand transport or variations of units origin, or age.

3.3.4. Amazonian sites

Amazonian aged volcanic plains displaying spectral signatures different than the nanophase ferric oxides typical of dust mantling were difficult to find. We have identified two small regions that display characteristics of volcanic plains (Fig. 5). The floor of Echus Chasma exhibits a very flat topography at MOLA scale. High Spatial Resolution Camera (HRSC) images show a surface with platy landforms, with a rough texture at the MOC scale, such as those observed for platy lava flows (e.g. Keszthelyi et al., 2000). This terrain has been dated recently as about 90 My by Chapman et al. (2007). It corresponds to the end of the young lava flows that flowed down the Tharsis area into the Kasei Vallis-Echus Chasma valley system, and dated to Late Amazonian (Scott and Tanaka, 1986). The region is broadly mantled by dust, but a dust-free window exists in the southern part of the Chasma as confirmed by the high thermal inertia reaching 520 TIU (Putzig et al., 2005) and its low albedo compared to mantled terrains. The pyroxenes detected here by OMEGA confirm the morphological interpretation of this canyon being filled by volcanic rocks. This area therefore enables us to retrieve the composition of a very young lava flows from the Tharsis region in a location devoid of massive sand sheets.

A terrain located on the floor of one of the Noctis Labyrinthus canyons consists of a flat area with low albedo and high thermal inertia from 300 to 630 TIU (Putzig et al., 2005). MOC and HRSC images show no aeolian landforms except a few dunes in the eastern edge of the floor. For the most part, there is a rough texture and local platy patterns (Mangold et al., 2008). This canyon floor was not known as a volcanic unit. The combination of strong pyroxene signatures by OMEGA, the absence of sand as seen from images and inertia, and the

flat topography of this unit favors the conclusion that this terrain corresponds to a volcanic filling of the canyon floor (Mangold et al., 2008). As this terrain was never identified as volcanic, we have derived an age from the impact craters seen at the surface. Crater counts give an age of several tens of My. This gives an additional composition of young lava flows of the Late Amazonian period in the Tharsis region.

4. Results

4.1. Derived modal mineralogy and particle size

Spectra representative of the diversity of the mafic regions are shown in Fig. 6. Overall, spectral fits using the nonlinear spectral mixing method are good (RMS <0.3%), suggesting that major mafic phases are well represented in the end-member library and they provide good fits to the surface types in this study. Small noticeable misfits between measured and some modeled spectra are observed at 1.3-1.6 μm and 2.4-2.5 μm. Their causes are not well understood but may result from an instrumental effect (small time-dependent deviations from linearity that depends on the flux received by the instrument), atmospheric effects, and/or precise end-member selection. However, it should not influence the mafic composition, which NIR diagnostic signatures are at different wavelengths. Moreover, the differences are smaller than 2%, which is on the order of the instrumental errors.

Most spectra were fit well with RMS error between measured and modeled spectra of less than 0.4%. As expected, the RMS increases with increasing albedo and exhibits values larger than 0.3% mainly for bright regions (Fig. 7). In order to restrict data to the low albedo terrains that contain the least amount of non-mafic components, in particular dust, modeled spectra with RMS values larger than 0.3% were excluded of the final evaluation of the modal mineralogy with the exception of the small Noctis Labyrinthus region, which has most values

larger than 0.4%. We indeed prefer to keep the modeling results about Noctis because it is one of the two alone Amazonian regions.

Derived mineralogy for each extended region is given in Table 2. The plagioclase abundance inferred by OMEGA is compared to a mineral group referred to as "neutral components", for which the abundance is the combined TES abundances of phases spectrally featureless in the NIR (plagioclase, high silica phases and quartz). The group referred to as "others" corresponds to Martian dust in the case of OMEGA, and to as diverse minerals (sulfates, carbonates…), whose the total abundance is below the detection limit in the case of TES. Apart from the olivine-rich terrains discussed below, we recall that the olivine abundance is given assuming forsterite as end-member and particle size fixed at 100 µm.

Plagioclase, HCP, LCP and Martian dust are in decreasing order of abundance, the dominant minerals for all the extended low albedo regions listed in Table 2. Plagioclase abundance always exceeds total pyroxene abundance. HCP abundance dominates over LCP one in all regions. Olivine is above the detection limit for one region only, Terra Tyrrhena, which is consistent with the olivine distribution inferred from spectral parameter mapping (Poulet et al., 2007). However, the average mineralogy determined for this region reflects a mixture of the regional composition with extended terrains that are enriched in olivine as shown in Poulet et al. (2007) rather than a homogeneous surface composition.

Modeled HCP and LCP abundances differ by 5-10% between regions. The mineralogy of the Hesperian Syrtis Major lavas is compared to Noachian unburied LCP-bearing highlands in the region around the Nili Fossae and to the localized LCP-bearing outcrops of the southern hemisphere (Table 3). The Syrtis lavas are depleted in LCP mineral in comparison to the older terrains. Note that the total pyroxene abundance exceeds plagioclase abundance in the localized LCP-bearing outcrops only.

The oxide derived abundance (magnetite) is in part controlled by the particle size of plagioclase (Fig. 6 of paper 1). For a plagioclase particle size of a few hundred micrometers, the magnetite abundance is of the order of 0.5 to 3%. Some variations of a few tenths of percent are seen from a region to region, but these differences are not significant given the uncertainties of the model.

The derived particle sizes are in the range of several tens to a few hundred micrometers (Fig. 8). Given the large uncertainties, no significant difference is observed between regions. However, we notice that the average HCP particle size is almost systematically larger than the average particle sizes of LCP and plagioclase minerals. Nevertheless, it is difficult to know if the particle size accounts for grain size in rocks or sand particles on the surface; the latter case is not directly related to the initial mineral size in rocks.

In the localized olivine-bearing terrains, the modal mineralogy is very diverse in terms of abundance and particle size (Table 4). Mg- and Fe-rich olivines are required for all the outcrops. The strong olivine signature detected in the region around the Nili Fossae shown in Fig. 6 (spot NFO) is best reproduced by large olivine particles >1 mm and abundance of ~40%. Such a large inferred particle size is unique among the studied regions. Additional minerals are plagioclase and HCP. LCP is also required for the olivine dunes in the caldera of Syrtis Major (SMN2). However, this LCP may come from the surrounding Syrtis Major lavas (SML) that contain LCP (Table 2), whereas the apparent enrichment of olivine in the dunes suggests that the source of the dune field is the olivine-bearing LCP-free eroded terrains (SMN1), consistent with the interpretation of Christensen et al. (2005). The mineralogy of these dunes represents a good example of mineralogy resulting from a compositional mixture of different types of terrains.

4.2 Classification

The mineralogies are classified by their normalized abundances of plagioclase, olivine, LCP and HCP on ternary diagrams (Figures 9 and 10), which represent two plans of the normative basalt tetrahedron (Streckeisen, 1976). The dust end-member, assumed not to be a component of the mafic rocks, is not used in the classification. The divisions between olivine-rich terrains and the rest of studied regions are evident in the ternary diagram displaying plagioclase, olivine, and pyroxene abundances (Fig. 9). Excluding the LCP-rich outcrops, which have a lower abundance of plagioclase, the olivine-poor regions are clustered in the middle of the plagioclase-pyroxene line corresponding to basaltic composition.

By contrast, region-to-region differences in modal mineralogy exist for the low-albedo olivine-free regions in the ternary diagram displaying mafic minerals (Fig. 10). While we note a restricted distribution along the LCP/HCP axis, the variations of LCP abundance show a compositional trend from the oldest terrains exhibiting the largest abundance (LCP-rich outcrops, Nili Fossae highlands) to the younger terrains having lesser abundance (early Hesperian volcanic provinces, and then recent Amazonian volcanic flows).

4.3. Comparison with previous remote sensing and in situ analyses

Overall, our derived abundances of plagioclase and HCP (40-60% plagioclase, 20-40% HCP) are close to the compositions of surface type 1 basalts derived from TES, which range from 45-60% neutral components and 25-35% HCP (Christensen et al., 2000a; Hamilton et al., 2001; Wyatt and McSween, 2002; McSween et al., 2003). We should bear in mind that the neutral components include plagioclase and high-silica phases (glass, sheet silicates and opal). Some of the TES analyses found that the total abundances of these phases divide into 35% plagioclase and 15-20% high silica phases. Given that the nature of the high-silica phases is still controversial (see discussion in paper 1), we nevertheless consider that

our assumption to compare the summed TES abundances of spectrally NIR featureless plagioclase and high-silica phases to the OMEGA abundance of plagioclase is valid for comparison purposes.

Because the regions are modeled as mixtures of similar mineral classes, a direct comparison with TES data from region-to-region is possible (Table 2). Except for Solis Lacus region, the bulk mineralogy of each region is remarkably consistent with that inferred from TES analyses in terms of HCP and plagioclase abundances (Rogers and Christensen, 2007). We emphasize that a 5-15% proportion of LCP is unambiguously required to model most of the low albedo OMEGA spectra. Small amounts of LCP pyroxenes (<10%) were reported in some low albedo regions by TES but are not above the detection limit (e.g. Bandfield, 2002). Occurrences of LCP above the TES detection limit were found by Rogers and Christensen (2007). Ongoing analysis of TES data also indicates that LCP may be widely distributed in the Noachian highlands and may provide a better assessment of its presence and detection limits (Hamilton and Koeppen, 2007). The properties of pyroxene-rich terrains on Mars identified in this study are qualitatively consistent with results from previous works obtained with the Modified Gaussian Model (MGM) for OMEGA data. For instance, the ancient terrains north of Syrtis Major indicate a relative enrichment in LCP while the younger Syrtis Major edifice exhibit terrains with the highest proportion of HCP (Kanner et al., 2007). However, the calculated LCP/(HCP+LCP) ratio (Table 2) quantitatively differs from modal abundances of the ancient Noachian terrains estimated from a normalized MGM band strength ratio (LCP/(LCP+HCP)) of OMEGA spectra (Kanner et al., 2007). The Noachian highlands exhibit a ratio of 0.40 in comparison to 0.59 in the Kanner et al. analyses.

Whereas the Solis Lacus region (acronym SL) is classified as a surface type 2 representative by TES (Bandfield, 2002), this region is a typical low albedo basaltic terrain based on our analysis. As explained previously, the northern low albedo regions were not

examined in this work mainly because the mafic signatures are very shallow, making uncertain the spectral modeling. To date, the best interpretation of the spectral signatures as seen by OMEGA is a dust- or rind-coated basaltic surface (Poulet et al., 2007). However, our model that simulates a granular surface cannot reproduce such a mixture. When this modeling issue is resolved, further comparisons to the TES results will be made.

TES globally mapped olivine abundances indicate that large expanses of the low albedo surface are characterized by olivine-bearing basalts in proportion of 10-15% (Christensen et al., 2000a; McSween et al., 2006a; Koeppen and Hamilton, 2008). Such abundance is here reported for Tyrrhena Terra only. OMEGA found a few other extended low albedo regions, not modeled here, but where olivine signatures similar to what we see in Tyrrhena Terra are detected (Poulet et al., 2007). This may indicate olivine in the same proportion than in Tyrrhena Terra, However, olivine is not present in most of the low albedo regions. It has been demonstrated that OMEGA is not sensitive to the presence of 10-15% (respectively 5-10%) of iron-poor olivine if the particle size is <<100 μm (resp. 100 μm) (Poulet et al., 2007; paper 1). However, the olivine end-members used in the TES deconvolution have large particle size (> 100 μm) and a pretty high content of iron (Fo~50-60), so that OMEGA should have detected a 10% abundance of such large particle-sized and iron-rich olivine. A possible explanation of this puzzling discrepancy may come from a weathering process that would preferentially alter olivine. The Microscopic Imager aboard the Mars Exploration Rover Spirit indeed revealed that tiny, irregular veins of light-colored material as well as surface rinds were uniquely present on the surface of olivine-rich rocks, suggesting that chemical weathering on Mars could preferentially alter olivine (McSween et al., 2006a). Mineralogical and chemical differences between Gusev rock surfaces and interiors further support this hypothesis, which is explained by the rapid dissolution of olivine under acidic conditions (Hurowitz et al., 2006). The weathered coating would then mask the

olivine signature in the NIR wavelength range, but not in the thermal range, indicative of a coating depth of a few micrometers at most. On the other hand, the higher olivine abundances (35-50%) found in the region around the Nili Fossae as well as the presence of HCP in proportion of 15-20% reported by different authors (Hoefen et al., 2003; Hamilton et al., 2003; Hamilton and Christensen, 2005; McSween et al., 2006a) are in excellent agreement with our estimate (Table 4).

A direct comparison of the mineralogy of Gusev rocks and soils with the OMEGA results cannot be done because the mineralogy of the landing site from remote sensing is mainly dominated by dust component, which masks the mafic mineral signatures (Lichtenberg et al., 2007). However, the composition of some Gusev rocks shares some similarities with that of the Nili Fossae olivine-rich deposits (NFO in Table 1). Different types of basalts are encountered near the Spirit rover landing site in Gusev Crater (Squyres et al., 2004b; Ruff et al., 2006; McSween et al., 2006a; 2006b; 2008), butnormative calculations suggest that some of these rocks (Adirondack, Humphrey, and Mazatzal) are basalts containing olivine with abundances up to 30% coexisting with pyroxene (30%) and plagioclase (40%). Microscopic images of these rocks give evidence for striking porphyric textures where olivine particles are millimeter-sized phenocrysts, which is also in good agreement with the olivine phenocrysts found in the region around the Nili Fossae. The typical OMEGA-derived mineralogy of the low albedo region (40-55% plagioclase, 30-40% pyroxenes, olivine <10%) agrees more with the composition of dark disturbed Gusev soils (50% plagioclase, 40% HCP, and 10% olivine from McSween et al. (2006a)). Conversely, other rocks that are mainly composed of sodic plagioclase (60%), pyroxenes, mostly hypersthene (10-30%) with some amounts of HCP, olivine and Fe-Ti-Cr oxides have no OMEGA analogue.

Finally, thermal inertia values for most of these regions range from ~150 to ~400 $J/m^2/K/s^{1/2}$, which corresponds to effective particle size ~50 to ~1000 μm based on the thermal inertia/particle size relationship (Presley and Christensen, 1997; Pelkey et al., 2001). The model match to sand-sized particles is thus consistent with the thermal inertia as well as infrared albedo values (Palluconi and Kieffer, 1981; Edgett and Christensen, 1991; Putzig et al., 2005).

4.4. Chemical composition and comparison with previous data

Chemistry is less diagnostic than modal mineralogy because one must make assumptions about the partitioning of elements into minerals and one must assume that there are no secondary phases present. Nevertheless, basaltic rocks are commonly classified by their chemistry because their petrographic texture makes it difficult to obtain modes. In this section, we therefore calculate wt% oxide composition from OMEGA-derived modal mineralogy using the mineral end-member compositions and densities (Table 5). We remark that the chemical compositions of the different end-members are out of equilibrium, and this is especially true for the olivine Fo 88 and the pyroxenes pigeonite and diopside. We recall that the selection of the end-members was driven by the fact that their optical properties (spectra and/or optical constants) were available. Regarding to the choice of olivine, Koeppen and Hamilton (2008) recently reported the mapping of 10-15% of olivine with Fo 53 and Fo 68 as the most dominant phases. Unfortunately, the optical constants of such olivines, which would be in equilibrium with the pyroxene minerals, are not available. From Poulet et al. (2007), we know that increasing the iron content of olivine and the grain size decreases the threshold of detection; we can deduce that the threshold of the Fo 50-60 olivine should be equal to something like 10% if the particle size is <<100 μm and to something like 5% for larger particle size. This means that the calculations of the chemical compositions, which use

an olivine abundance of 5% at most (see next paragraph), could be also applied to the type of olivine detected by TES. Regarding to the choice of the pyroxenes, paper 1 has shown that significant differences in terms of chemical compositions do not affect strongly the NIR properties of pyroxenes. Indeed, the diposide can be replaced by an augite, which contains a significant higher content of iron (18% instead of 8%, see Table 5) without the modal mineralogy being significantly different (Poulet et al., 2008). That said, we believe that a further work will be to recalculate the modal mineralogy and thus the chemical compositions from new minerals in equilibrium, when optical constants of these minerals will be available. This case prompts us to bear in mind that reflectance spectroscopy alone may lead to intrinsic ambiguities in terms of chemical composition and petrology.

The chemical analyses with their uncertainties of eleven regions are summarized in Table 6. For these calculations, we assume the iron-poor HCP diopside, a 2.5+/-2.5 vol % abundance of Fo 88, and a 2+/-1% of magnetite. Uncertainties on the modal composition of each mineral have been propagated to chemical composition. In particular, a balance between the abundance of plagioclase and those of mafics (LCP, HCP, olivine) is assumed as following: higher abundance of plagioclase corresponds to a lower abundance of mafics, and vice versa.

In the FeO* / MgO vs. SiO_2 diagram (Fig. 11), the OMEGA-derived chemical analyses are plotted near the origin of both tholeiitic and subalkaline fractionation paths. With respect to modal uncertainties, this location in the diagram is not diagnostic in terms of crystal fractionation trend. In the same way, we cannot discriminate between dry and hydrous melting peridotite.

SiO_2 contents are ranged between 48.5 and 50% (Table 6). As illustrated in Fig. 11, these contents are significantly less than the values obtained by TES-derived compositions including both type 1 and type 2 surfaces (Bandfield et al., 2000; Hamilton et al., 2001;

McSween et al., 2003). Al_2O_3 contents are between 15 and 18%, and CaO contents between 12. and 15%. Al_2O_3 values are close to the values derived from TES, while the CaO contents are significantly larger (McSween et al, 2003). These observed discrepancies could partly come from the fact that plagioclase used in our calculation is rather Ca-rich (labradorite).

The OMEGA data, although slightly silica richer than olivine-rich basalts at Gusev Crater, are nevertheless more consistent with these in situ measurements than TES results. The SiO_2 content is also quite consistent with the global Gamma Ray Spectrometer (GRS) data (Boynton et al., 2007). By contrast, the calculated FeO* / MgO ratio is lower than those found for the Gusev rocks. It is also smaller than the GRS data, which show that none of the 5x5 degree grid points have FeO smaller than about 12 wt. %, with a peak in the values at about 18 wt. % (Taylor et al., 2006). The OMEGA-derived FeO* / MgO ratio, and especially the iron content, is very dependent on the total iron oxide content, which is not well constrained by our approach. In particular, the content is a function of the particle size of plagioclase. We also note that our calculations shown in Table 6 assume a 2.5% abundance of Fo 88, the iron-poor diopside, and a 2% of magnetite. This case corresponds to a lower limit of iron content. We therefore calculate a new estimate of the chemical composition of one of low albedo regions (Terra Meridiani, where a modeling test starting with augite instead of diopside as the HCP end-member was successfully done in paper 1) by assuming new hypotheses: augite is used instead of diopside, and an abundance of the olivine Fo 88 is fixed at 10+/-5% (such olivine abundance can be present if the particle size is <<100 μm). In this case, the total iron content increases to 12+/-1 wt%, and the ratio FeO* / MgO to ~1.1 (note that the SiO_2 content does not change). These values are closer to the GRS and in situ measurements, but still smaller. Therefore, the only way to increase the iron content is to increase the content of iron oxide. This implies that a next set of derivation of modal

mineralogy should be implemented by forcing a higher iron oxide content (~8-10%) during the spectral modeling step.

Terrestrial lava ferropicrite analyses (Hanski and Smolkin, 1989) have been also plotted in the same diagram for comparison. Although the FeO* / MgO ratio is similar to ferropicrites, the Mars surface compositions are slightly enriched in silica. However, ferropicritites have nearly the same SiO_2 content compared to Gusev rocks. Note finally that the specific Pathfinder data (not plotted) are totally different from OMEGA results as they are silica-richer (57 wt. % SiO_2) with a very high FeO*/MgO ratio (McSween et al., 1999; Foley et al., 2003).

4.5. Comparison with Martian meteorites

Quite a number of Martian meteorites namely the Nakhlites, the Chassignites ALH86001 and lherzolitic Shergottites are partial cumulate rocks. Their compositions do not represent anymore the initial magma from which they derived due to fractionation. This also implies that the parent materials may not be widely distributed on the uppermost surface, even if they reside within the few meters of the surface. Our work shows that the pyroxene- and olivine-rich compositions of the majority of the meteorites are indeed not well matched by the typical basaltic surface composition of the low albedo regions. We however identified a good correlation between the modal mineralogy inferred for Nili Fossae (NFO) with the composition of olivine-bearing materials ressembling ALH77005 and Chassigny (Fig. 13).

We now focus our comparison on iron rich basaltic Shergottites and olivine phyric Shergottites that do show basaltic texture. The modal mineralogy of areas analyzed here clearly indicates an affinity with some of the basaltic Shergottites (Fig. 12). However, the calculated plagioclase amounts (40-50 %) are close to the maximum values found in basaltic Shergottites (Goodrich et al., 2003). Most of basaltic Shergottites are LCP-richer than the

OMEGA analyzed areas (Fig. 13). Proportions of these two pyroxenes have not been reported for all Shergottites, but those with measured modal abundances have proportions that range from 1:1 to 18:1 (e.g., Stolper and McSween, 1979; McSween and Jarosewich, 1983; Treiman et al., 1994; Hale et al., 1999; Zipfel et al., 2000; Barrat et al., 2002; Taylor et al., 2002; Goodrich et al., 2003). Picritic Shergottites are plagioclase poor compared to picritic basalt from Gusev and olivine-rich terrains from Syrtis Major and Nili Fossae. More generally, from all modal data, an evolution (Fig. 12) could be evidenced from picritic Shergottites, to basaltic Shergottites, to mafic scanned areas.

Basaltic Shergottite chemical analyses compiled by McSween et al. (2003) are plotted in the FeO* / MgO vs. SiO_2 diagram (Fig. 11). The OMEGA derived SiO_2 contents are in the range of values found in basaltic Shergottites. By contrast, the FeO* / MgO ratios are relatively lower.

5. Discussion

5.1. Implications for the Martian mantle

Spectroscopic analyses made by OMEGA and TES have the advantage of providing a way to study Mars' surface composition at the planetary scale. However incomplete and restricted mineral inventories (plagioclase, pigeonite, diopside, and olivine, where oxides are tied to plagioclase, or vice versa) provide only partial constraints on petrogenesis. Moreover, we must be careful in the interpretation of the OMEGA derived modal compositions because the mineralogical differences could result from the heterogeneity of the scanned area. Although the geomorphologic properties of the study areas seem to indicate that we sample extrusive lava flows (section 3.3), we cannot totally exclude that the observed variations of the ratios between plagioclase and pyroxene, and between HCP and LCP, could be governed

by mechanical erosion, chemical alteration, mechanical sorting, and/or distribution of the outcrops and sand deposits.

Despite these uncertainties, the low albedo surface compositions seen by OMEGA are characterized by a basaltic composition, a lower amount of SiO_2 than in the TES data, a restricted distribution and an evolution through time of the HCP/LCP ratio, and significant variations of the olivine abundance. These characteristics as well as the analogy with some terrestrial rocks and Gusev rocks are discussed in the following paragraphs.

(i) OMEGA chemical derived analyses indicate a basaltic composition for all of the low albedo extended regions. They are quite consistent with Gusev in situ data and Shergottite compositions but they appear to be significantly SiO_2-poorer than TES data. McSween et al. (2003) proposed two alternative hypotheses to explain the respective andesite-basalt and andesite TES-derived surfaces type 1 and type 2: (1) hydrous melting and fractional crystallization; (2) weathering of basalts, which leads to mobility of silica. Our results indicate that sediments associated with ancient Martian crust are basaltic without discarding tholeiitic affinities in opposition to the TES-derived andesitic composition. Such a composition obviates the need to appeal to hydrous melting or weathering of basaltic rocks, and it is consistent with the conventional view of Mars as having a relatively dry mantle and no plate tectonics. Note finally that the conclusion about a dry mantle with no plate tectonics is also reinforced by recent analyses of the GRS data (Taylor et al., 2006).

(ii) Most of calculated modal compositions are dominated by plagioclase, pyroxenes (HCP and LCP, with HCP≥LCP) and minor amounts of olivine (Figures 9 and 10). This modal mineralogy is typical of mafic magmatic rocks, which could be classified as gabbro-norites with minor amount of olivine for plutonic rocks; the

volcanic equivalent nomenclature is two-pyroxene basalt. The Noachian-aged outcrops exhibit the largest amount of LCP and the lowest amount of plagioclase. The high content of pigeonite (LCP end-member) in magmatic rocks might correspond to partial melting under significant H_2O partial pressure (Dann et al., 2001; McSween et al., 2001). Accordingly, the LCP-rich outcrops could have been formed from H_2O-bearing melts. The other studied terrains, corresponding to lava flows, are characterized by a decreasing LCP absolute amount with time, reflecting a decrease of the Mg/Ca ratio. This LCP/HCP relative variation can be explained by a decreasing degree of partial melting as thermal flux is expected to decrease with time. The partial melting decrease leads to a decrease of the silica activity and a drop-off of the LCP content.

In summary, we propose that the most ancient terrains enriched in LCP to the detriment of plagioclase, could have been formed through melting under significant H_2O partial pressure. Then, dry, basaltic volcanism occurred leading to decreasing LCP amount with time due to decreasing degree of partial melting.

(iii) We only found scarce evidence of olivine-rich basalts (picritic basalt or troctolite type rock), although they are frequently detected at Gusev crater. In the region around the Nili Fossae, millimeter-sized particles are modeled. Again, if olivine phenocrysts were present in the extended low albedo regions, they should have been detected by OMEGA and calculated abundance would have been retrieved accordingly. This suggests that most areas analyzed by OMEGA are more evolved than picritic basalt and have been fractionated. If the rocks are confirmed to be olivine-poor, they would correspond to significantly differentiated magmas, after a significant time of residence inside the crust. Conversely, olivine-rich terrains with phenocrysts found in Nili Fossae could therefore witness primitive magmas.

Alternatively, formation by impact is also a possible formation process (Mustard et al., 2007).

(iv) The average modal mineralogy of the studied regions has some similarities with the composition of terrestrial rocks. Most of the studied areas correspond to the modal compositions observed in the well known plutonic mafic-ultramafic complexes such as Bushveld complex, South Africa (Irvine and Sharpe, 1982), or Palisades Sill, USA (Shirley, 1987). In these complexes, gabbros-norites are plagioclase-rich and contain two types of pyroxenes and minor olivine content. Volcanic equivalent is two-pyroxene basalt. However, pigeonite-augite association is not frequent in terrestrial rocks, which usually contain orthopyroxene-augite association (Wager and Brown, 1968). As mentioned previously, the best explanation so far of the presence of pigeonite instead of orthopyroxene would be a significant partial pressure of H_2O in the mantle source.

Iron-rich ferropicrite from Baltic shield of Kola Peninsula are proterozoic hot spot generated primitive volcanics. The iron-rich character of the lava directly reflects an iron anomaly in the mantle source region rather than being the result of a differentiation process. It could be a good analogue of the Martian mantle for several reasons: (1) the Martian mantle is interpreted to be enriched in iron compared to the terrestrial mantle (Dreibus and Wänke, 1985); (2) this plume generated volcanism is independent of plate tectonics; (3) it had been generated in proterozoic time where the heat flow, thus the degree of partial melt, was higher compared to more recent type of volcanism. In FeO* / SiO_2 diagram ferropicrites are SiO_2-poor, which corresponds to their picritic character. Although the OMEGA data are close to the ferropicrite field, there is still a noticeable difference in SiO_2 content. This larger content in OMEGA data is in good agreement with the

low abundance of olivine. The observed difference between the OMEGA-derived composition and the ferropicrite composition would thus imply a slow fractionation that occurred possibly during a slow ascent as already inferred in the previous point. Moreover, we report a large discrepancy of iron content between our analysis and the ferropicrites. Our best explanation is that our modeling underestimates the abundance of the dark iron oxide (magnetite) by several percent.

5.2. Implications for Martian meteorites

SNC meteorites are essentially intrusive coarse-grained cumulate rocks except for picritic Shergottites that looks like Gusev effusive rocks. It is important to note that olivine is nearly present in all classes of SNC meteorites except for basaltic Shergottites. In lherzolitic Shergottites and Chassignites, olivines are cumulate magnesium-rich crystals, while in picritic Shergottite and Nakhlites they form iron–rich zoned megacryst, and their origin (phenocryst vs xenocrysts) is still a debatable issue. Our OMEGA-based analysis indicates that olivine with large mm-sized iron-rich olivine is abundant in Nili Fossae. These terrains are rather good analogues to the olivine-bearing meteorites (ALH77005 and Chassigny) as first noted by Hamilton et al. (2003).

Shergottites are usually dated as recent magmatic rocks formed between 175 and 475 Ma (Nyquist et al., 2001 and references therein). This suggests that they are representative of last volcanic stages on Mars. Unfortunately, the youngest volcanic plains are blanketed by dust not enabling any orbital data to retrieve their composition. This leads Hamilton et al. (2003) to conclude that spectral data of these regions are not able to be compared to most SNC meteorites for this reason. In our study, we identified and determined the composition of two spots of non mantled recent lava flows of the Late Amazonian, with ages as young as 90

to 100 My (section 3.3.4). These ages are in the same range as the Shergottites. However, the composition of these two spots is the farthest from the composition of Shergottites in term of LCP/HCP ratio: these spots are the areas the most enriched in HCP over all studied areas. This does not exclude that other regions of recent volcanic activity have different ratios. However, the fact that these lava plains are different from the composition of basaltic Shergottites, together with the fact that the observed trend in LCP/HCP ratio favors a decrease of the LCP occurrence through time, is difficult to reconcile with the young age of Shergottites. The alternative ages found recently by Bouvier et al. (2005, 2008) of about 4.0 Gy for Shergottites would better fit our analysis. This would explain at the same time that the Shergottites are different from the young lava flows, whereas ancient crustal rocks in the locations studied here are much closer to their composition.

6. Conclusion

OMEGA/MEx reflectance spectra are used to derive the modal mineralogy of diverse Martian mafic regions and to identify spatial trends in mineralogical assemblages. The studied regions primarily consist of plagioclase, HCP- and LCP- pyroxenes, and minor amount of olivine. This mineralogy is typical of gabbro-norites and volcanic two pyroxene basalts. The calculated particle sizes are in the range of a few hundred micrometers, which is consistent with the thermal inertia derived from infrared observations. The highest concentrations of LCP and the lowest amount of plagioclase inferred are associated with the most ancient terrains. Olivine abundance is found to be relatively high in localized areas only (Syrtis Major Patera and Nili Fossae). Particle sizes larger than 1 mm are modeled in Nili Fossae. This corresponds to typical troctolite type rock or picritic basalt.

OMEGA is a mineralogical tool, but it can also provide a means of estimating chemistry. Our chemical analyses indicate a basaltic composition for all low albedo extended

regions. They are quite consistent with GRS data, Gusev in situ data and basaltic Shergottite compositions in term of SiO_2 content, and they appear to be significantly SiO_2-poorer than TES data. By contrast, the derived bulk total Fe contents ($FeO+Fe_2O_3$) are way smaller than soil and rock analyses from GRS and in situ measurements. The discrepancy could be partly explained by the assumptions used for our calculations (abundances and iron content of the olivine and HCP end-members). However, the only way to significantly increase the iron content would be to increase the content of iron oxide, which is not well constrained, because it depends on the particle size of the plagioclase end-member. This implies that a set of spectral modeling should be implemented by forcing a higher iron oxide content of ~8-10%.

The composition of the Noachian-aged, LCP-rich outcrops could trace crystallization under significant H_2O partial pressure conditions. Mantle water being thought to be magmatic (McSween et al., 2001), leads to an early crust enriched in LCP with later drier, basaltic volcanism. The evolution to HCP-richer basaltic lava flows with time is interpreted to be a consequence of decreasing of partial melting as thermal flux decreases with time.

Martian meteorites have young crystallization ages, suggesting that they are samples of young (dust-covered) volcanic centers such as Tharsis or Elysium. On the basis of a comparison of the OMEGA-based Mars surface composition with those of basaltic Shergottites, it appears that these meteorites could be witness of much older Martian magmas. The observed trend in LCP/HCP ratio, which favours a decrease of the LCP abundance through time, is indeed difficult to reconciliate with the young age of Shergottites. An older age (possibly 4.0 Gy) would explain at the same time that the young lava flows are different from Shergotittes, whereas ancient crustal rocks are much closer to their composition. The picritic basalt composition inferred in the region around the Nili Fossae is similar to the olivine-bearing material resembling ALH77005 and Chassigny.

References

Arvidson, R.E., Seelos, F.P., Deal, K.S., Koeppen, W.C., Snider, N.O., Kieniewicz, J.M., Hynek, B.M., Mellon, M.T., Garvin, J.B. 2003. Mantled and exhumed terrains in Terra Meridiani, Mars. J. Geophys. Res. 108, doi:10.1029/2002JE001982.

Arvidson, R.E., and 24 colleagues, 2006. Nature and origin of the hematite-bearing plains of Terra Meridiani based on analyses of orbital and Mars Exploration rover data sets. J. Geophys. Res. 111, doi:10.1029/2006JE002728.

Bandfield, J.L., Hamilton, V.E., Christensen, P.R., 2000. A global view of Martian surface compositions from MGS-TES. Science 287, 1626–1630.

Bandfield, J.L., 2002. Global mineral distributions on Mars. J. Geophys. Res. 107(E6), doi:10.1029/2001JE001510.

Bandfield, J.L., Christensen, P.R., Hamilton, V.E., McSween, H.Y., Jr., 2002. Global mineral distributions on Mars. J. Geophys. Res. 107(E6), doi:10.1029/2001JE001510.

Barrat, J. A., Jambon, A., Bohn, M., Gillet, P., Sautter, V., Gopel, C., Lesourd, M., Keller, F., 2002. Petrology and chemistry of the pricritic shergottite NorthWest Africa 1068(NWA 1068). Geochim. Cosmochim. Acta 66, 3505-3518.

Baratoux, D., Pinet, P., Gendrin, A., Kanner, L., Mustard, J., Daydou, Y., Vaucher, J., Bibring, J.-P., 2007. Mineralogical structure of the subsurface of Syrtis Major from OMEGA observations of lobate ejecta blankets. J. Geophys. Res. 112, doi:10.1029/2007JE002890.

Bell, J.F., Wolff, M.J., James, P.B., Clancy, R.T., Lee, S.W., Martin, L.J., 1997. Mars surface mineralogy from Hubble Space Telescope imaging during 1994–1995: Observations, calibration, and initial results. J. Geophys. Res. 102(E4), 9109-9123.

Bibring, J.-P., et al. (2004), OMEGA: Observatoire pour la Minéralogie, l'Eau, les Glaces et l'Activité, in Mars Express: The Scientific Payload, edited by A.Wilson, Eur. Space Agency Spec. Publ., ESA-SP 1240, 37– 49.

Bibring, J.-P., Langevin, Y., Gendrin, A., Gondet, B., Poulet, F., Berthe, M., Soufflot, A., Arvidson, R.E., Mangold, N., Mustard, J.F., Drossart, P., Omega Team, 2005. Mars surface diversity as revealed by the OMEGA/MarsExpress observations. Science 307, 1576–1581.

Bouvier, A., Blichert-Toft, J., Vervoort, J. D., Albarède, 2005. The age of SNC meteorites and the antiquity of the Martian surface. Earth Planet. Sci. Lett. 240, 221-233.

Bouvier, A., Blichert-Toft, J., Vervoort, J. D., Gillet, P., Albarède, F., 2008. The case for old basaltic shergottites. Earth Planet. Sci. Lett. 266, 105-124.

Boynton, W. V., et al., 2007. Concentration of H, Si, Cl, K, Fe, and Th in the low- and mid-latitude regions of Mars, J. Geophys. Res. 112(E12S99), doi:10.1029/2007JE002887.

Chapman M.G., Neukum, G., Werner, S. C., van Gasselt, S., Dumke, A., Zuschneid, W., Michael, G., 2007. Echus Chasma And Kasei Valles, Mars: New Data And Geologic Interpretations. Lunar Planet. Sci. Conf. 38th, abst. 1407.

Christensen, P.R., Bandfield, J.L., Smith, M.D., Hamilton, V.E., Clark, R.N., 2000a. Identification of a basaltic component on the martian surface from Thermal Emission Spectrometer data. J. Geophys. Res. 105(E4), 9609–9621.

Christensen, P.R., and 15 colleague, 2000b. Detection of crystalline hematite mineralization on Mars by the Thermal Emission Spectrometer: Evidence for near-surface water. J. Geophys. Res. 105(E4), 9623– 9642.

Christensen, P.R, and 25 colleagues, 2001. Mars Global Surveyor Thermal Emission Spectrometer experiment: Investigation description and surface science results. J. Geophys. Res. 111, E02S10, doi:10.1029/2005JE002477.

Christensen, P.R, and 26 colleagues, 2004. Mineralogy at Meridiani Planum from the Mini-TES Experiment on the Opportunity Rover. Science 306, 1730-1733.

Christensen, P.R., McSween, H.Y., Bandfield, J.L., Ruff, S.W., Rogers, A.D., Hamilton, V.E., Gorelick, N., Wyatt, M.B., Jakosky, B.M., Kieffer, H.H., Malin, M.C., Moersch, J.E., 2005. Evidence for magmatic evolution and diversity on Mars from infrared observations. Nature 436, 504-509.

Cloutis, E.A., Gaffey, M.J., 1991. Pyroxene spectroscopy revisited: Spectral compositional correlations and relationship to geothermometry. J. Geophys. Res. 96, 22809–22826.

Dann, J.C., Holzheid, A.H., Grove, T.L., McSween, H.Y., Jr., 2001. Phase equilibria of the Shergotty meteorite: Constraints on pre-eruptive water contents of martian magmas and fractional crystallization under hydrous conditions. Meteoritics & Planetary Science 36, 793-806.

Dreibus, G., Wänke, H., 1985. Mars : a voltaile-rich planet. Meteoritics 20, 367-382.

Dreibus, G., Spettel, B., Haubold, R., Jochum, K. P., Palme, H., Wolf, D., Zipfel, J., 2000. Chemistry of a new shergottite: Sayh Al Uhaymir 005. Meteorit. Planet. Sci. 35, A49.

Edgett, K.S., Christensen, P.R., 1991. The particle size of Martian aeolian dunes. J. Geophys. Res. 96, 22,765–22,776.

Foley, C.N. Economou, T., Clayton, R.N., 2003. Final chemical results from the Mars Pathfinder alpha proton X-ray spectrometer. J. Geophys. Res. 108(E12), doi:10.1029/2002JE002019.

Folco, L., Franchi, I.A., D'Orazio, M., Rocchi, S., Schultz, L., 2000.A new Martian meteorite from the Sahara: The shergottite Dar al Gani 489. Meteorit. Planet. Sci. 35, 827– 839.

Gendrin, A., Mangold, N., Bibring, J.-P., Langevin, Y., Gondet, B., Poulet, F., Bonello, G., Quantin, C., Mustard, J., Arvidson, R., LeMouélic, S., 2005. Sulfates in Martian Layered Terrains: The OMEGA/Mars Express View. Science 307, 1587-1591.

Goodrich, C.A., Herd, C.D.K., Taylor, L.A., 2003. Spinels and oxygen fugacity in olivine-phyric and lherzolitic shergottites. Meteoritics &Planetary Science 38, 1773-1792.

Greeley, R., Guest, J.E., 1987. Geologic map of the Eastern Equatorial Region of Mars, scale 1:15,000,000. U.S.G.S. Misc. Inv. Series Map I-1802-B.

Hale, V.P.S., McSween, H.Y., McKay, G.A., 1999. Re-evaluation of intercumulus liquid composition and oxidation state for the Shergotty meteorite, Geochim. Cosmochim. Acta 63, 1459-1470, 1999.

Hamilton, V.E., Wyatt, M.B., McSween, H.Y., Christensen, P.R. 2001. Analysis of terrestrial and Martian volcanic compositions using thermal emission spectroscopy: 2. Application to Martian surface spectra from MGS TES. J. Geophys. Res. 106, 14,733-14,746.

Hamilton, V.E., Christensen, P.R., McSween, H.Y., Jr., Bandfield, J.L. 2003. Searching for the source regions of Martian meteorites using MGS TES: Integrating Martian meteorites into the global distribution of igneous materials on Mars. Meteorit. Planet. Sci. 38, 871-886.

Hamilton, V.E., Christensen, P.R., 2005. Evidence for extensive, olivine-rich bedrock on Mars. Geology 33(6), 433-436.

Hamilton, V.E., Koeppen, W.C., 2007. Global Mineral Maps of Mars: Examination of Compositional Variation Within Solid Solution Series. American Geophysical Union, Fall Meeting 2007, abstract #P13D-1549.

Hanski, E.J., Smolkin, V.F., 1989. Pechenga ferropicrites and other Early Proterozoic picrites in the eastern part of the Baltic Shield. Precambrian research 45, 1-3, 63-82.

Hiesinger, H., Head, J.W., 2004. The Syrtis Major volcanic province, Mars: Synthesis from Mars Global Surveyor data. J. Geophys. Res. 109, E01004, doi:10.1029/2003JE002143.

Hoefen, T.M., Clark, R.N., Bandfield, J.L., Smith, M.D., Pearl, J.C., Christensen, P.R., 2003. Discovery of Olivine in the Nili Fossae Region of Mars. Science 302, 627-630.

Hurowitz, J.A., McLennan, S.M., Tosca, N.J., Arvidson, R.E., Michalski, J.R., Ming, D.W., Schröder, C., Squyres, S.W., 2006. In situ and experimental evidence for acidic weathering of rocks and soils on Mars. J. Geophys. Res. 111, E02S19, doi: 10.1029/2005JE002515.

Ikeda, Y., Kimura, M., Takeda, H., Shimoda, G., Kita, N. T., Morishita, Y., Suzuki A., Jagoutz, E., Dreibus G., 2006. Petrology of a new basaltic shergottite: Dhofar 378. Antarctic Meteorite Res. 19, 20-44.

Imae, N., Ikeda, Y., Shinoda, K., Kojima, H., Iwata, N., 2003.Yamato nakhlites: Petrography and mineralogy. Antarct. Meteorite Res. 16, 13-33.

Irvine, T.N., Sharpe, M.R., 1982. Source-rock compositions and depths of origin of Bushveld and Stillwater magmas. Yb. Carnegie Inst. Wash. 81, 294−303.

Koeppen, W.C., Hamilton, V.E., 2008. Global distribution, composition, and abundance of olivine on the surface of Mars from thermal infrared data, J. Geophys. Res., 113, E05001, doi:10.1029/2007JE002984.

Kanner, L.C., Mustard, J.F., Gendrin, A., 2007. Assessing the limits of the Modified Gaussian Model for remote spectroscopic studies of pyroxenes on Mars. Icarus 187, 442–456.

Keszthelyi, L., McEwen, A.S., Thordarson, T., 2000. Terrestrial analogs and thermal models for martian flood lavas. J. Geophys. Res. 105, 15027-15049.

Kieffer, H.H., Martin, T.Z., Peterfreund, A.R., Jakosky, B.M., Miner, E.D., Palluconi, F.D. 1977. Thermal and albedo mapping of Mars during the Viking primary mission, J. Geophys. Res. 82, 4249–4291.

Langevin, Y., Bibring, J.-P., Montmessin, F., Forget, F., Vincendon, M., Douté, S., Poulet, F., Gondet, B., 2007. Observations of the south seasonal cap of Mars during recession in 2004–2006 by the OMEGA visible/near-infrared imaging spectrometer on board Mars Express. J. Geophys. Res. 112, E08S12, doi:10.1029/2006JE002841.

Lichtenberg, K. A., et al., 2007. Coordinated analyses of orbital and Spirit Rover data to characterize surface materials on the cratered plains of Gusev Crater, Mars. J. Geophys. Res. 112, E12S90, doi:10.1029/2006JE002850.

Lodders, K., 1998. A survey of shergottite, nakhlite and chassigny meteorites whole-rock compositions. Meteorit. Planet. Sci. 22, A183– A190.

Mangold, N., Allemand, P., Thomas, P.G., Vidal, G., 2000. Chronology of compressional deformation on Mars: evidence for a single and global origin. Planetary and Space Science 48, 1201-1211.

Mangold, N., Poulet, F., Mustard J. F., Bibring, J.-P., Gondet, B., Langevin, Y., Ansan, V., Masson, Ph., Fassett, C., Head J. W. III, Hoffmann, H., Neukum, G., 2007. Mineralogy of the Nili Fossae region with OMEGA/Mars Express data: 2. Aqueous alteration of the crust. J. Geophys. Res. 112, E08S04, doi:10.1029/2006JE002835.

Mangold N., Gendrin, A., Gondet, G,. Le Mouélic, S., Quantin, C., Bibring, J.-P., Langevin, Y., Poulet, F., Ansan, V., Masson, Ph., Hauber, E., Neukum, G., the OMEGA and HRSC Co-Investigator Teams, 2008. Mineralogy of west tithonium chasma-noctis labyrinthus, mars: putative volcanism on Noctis canyon floors. Lunar and Planetary Science Conference 39th, Abstract 1592.

McCord, T.B., Clark, R.N., Huguenin, R.L., 1978. Mars - Near-infrared spectral reflectance and compositional implication. J. Geophys. Res. 83, 5433-5441.

McSween, H.Y., Jarosewich, E., 1983. Petrogenesis of the Elephant Moraine A79001 meteorite Multiple magma pulses on the shergottite parent body. Geochimica et Cosmochimica Acta 47, 1501-1513.

McSween, H.Y., Eisenhour, D. D., Taylor, L. A., Wadhwa, M., Crozaz, G., 1996. QUE94201 shergottite: Crystallization of a Martian basaltic magma. Geochim. Cosmochim. Acta 60, 4563-4569.

McSween, H.Y., et al., 1999. Chemical, multispectral and textural constraints on the composition and origin of rocks at the Mars Pathfinder landing site. J. Geophys. Res. 104, 8679-8715.

McSween, H. Y., Grove, T. L., Lentz, R. C. F., Dann, J. C., Holzheid, A. H., Riciputi, L. R., Ryan, J. G., 2001. Geochemical evidence for magmatic water within Mars from pyroxenes in the Shergotty meteorite. Nature 409, 487-490.

McSween, H.Y., Jr., Grove, T.L., Wyatt, M.B., 2003. Constraints on the composition and petrogenesis of the Martian crust. J. Geophys. Res. 108(E12), 5135, doi:10.1029/2003JE002175.

McSween, H.Y., Jr., and 41 colleagues, 2006a. Characterization and petrologic interpretation of olivine-rich basalts at Gusev Crater, Mars. J. Geophys. Res. 111, E02S10, doi:10.1029/2005JE002477.

McSween, H.Y., Jr., and 13 colleagues, 2006b. Alkaline volcanic rocks from the Columbia Hills, Gusev crater, Mars. J. Geophys. Res. 111, Issue E9, doi:10.1029/2006JE002698.

McSween, H.Y., Jr., and 14 colleagues, 2008. Mineralogy of volcanic rocks in Gusev Crater, Mars: Reconciling Mössbauer, Alpha Particle X-Ray Spectrometer, and Miniature Thermal Emission Spectrometer spectra. J. Geophys. Res. 113, E06S04, doi:10.1029/2007JE002970.

Meyer, C., 2008. The Mars Meteorite Compendium. Astromaterials Research & Exploration Science (ARES) (JSC #27672 Revision C) Lyndon B. Johnson Space Center Houston, Texas, http://curator.jsc.nasa.gov/antmet/mmc/index.cfm.

Mustard, J.F., Erard, S., Bibring, J.-P., Head, J.W., Hurtrez, S., Langevin, Y., Pieters, C.M., Sotin, C.J., 1993. The surface of Syrtis Major - Composition of the volcanic substrate and mixing with altered dust and soil. J. Geophysic. Res. 98(E2), 3387-3400.

Mustard, J.F., Murchie, S., Erard, S., Sunshine, J. M., 1997. In situ compositions of martian volcanics: Implications for the mantle. J. Geophys. Res. 102, 25605–25615.

Mustard, J.F., Poulet, F., Gendrin, A., Bibring, J.-P., Yangevin, Y., Gondet, B., Mangold, N., Bellucci, G., Altieri, F., 2005. Olivine and pyroxene diversity in the crust of Mars. Science 307, 1594–1597.

Mustard, J. F., Poulet, F., Head, J. W., Mangold, N., Bibring, J.-P., Pelkey, S. M., Fassett, C. I., Langevin, Y., Neukum, G., 2007. Mineralogy of the Nili Fossae region with OMEGA/Mars Express data: 1. Ancient impact melt in the Isidis Basin and implications for the transition from the Noachian to Hesperian. J. Geophys. Res. 112, E08S03, doi:10.1029/2006JE 002834.

Nyquist, L.E., Bogard, D.D., Shih, C.-Y., Greshake, A., Stöffler, D., Eugster, O., 2001. Ages and Geologic Histories of Martian Meteorites. Space Science Reviews 96 105-164.

Palluconi, F.D., Kieffer, H.H, 1981. Thermal inertia mapping of Mars from 60°S to 60°N. Icarus 45, 415–426.

Pelkey, S.M., Jakosky, B.M., Mellon, M.T., 2001. Thermal inertia of crater-related wind streaks on Mars. J. Geophys. Res. 106(E10), 23909-23920.

Pinet, P., Chevrel, S., 1990. Spectral identification of geological units on the surface of Mars related to the presence of silicates from earthbased near-infrared telescopic CCD imaging. J. Geophys. Res. 95(B9), 14435-14446.

Poulet, F., Cuzzi, J. N., Cruikshank, D. P., Roush, T., Dalle Ore, C. M., 2002. Comparison between the Shkuratov and Hapke Scattering Theories for Solid Planetary Surfaces: Application to the Surface Composition of Two Centaurs. Icarus 160(2), 313-324.

Poulet, F., Mangold, N., Erard, S., 2003. A new view of dark Martian regions from geomorphic and spectroscopic analysis of Syrtis Major. Astronomy and Astrophysics 412, L19–L23.

Poulet, F., Erard, S., 2004. Nonlinear spectral mixing: Quantitative analysis of laboratory mineral mixtures. J. Geophys. Res. 109(E2), doi:10.1029/2003JE002179.

Poulet, F., Bibring, J.-P., Mustard, J.F., Gendrin, A., Mangold, N., Langevin, Y., Arvidson, R.E., Gondet, B., Gomez, C., 2005. Phyllosilicates on Mars and implications for early martian climate. Nature 438, 623-627.

Poulet, F., Gomez, C., Bibring J.-P., Langevin, Y., Gondet, B., Pinet, P., Belluci, G., Mustard, J.F., OMEGA team, 2007. Martian surface mineralogy from OMEGA/MEx: Global mineral maps. J. Geophys. Res. 112, E08S02, doi:10.1029/2006JE002840.

Poulet, F., Bibring, J.-P., Langevin, Y., Mustard, J. F., Mangold, N., Vincendon, M., Gondet, B., Pinet, P., Bardintzeff, J.-M., Platevoet, B., 2008. Quantitative compositional analysis of Martian mafic regions using MEx/OMEGA reflectance data: 1. Methodology, uncertainties and examples of application. (Paper 1). Icarus moderate revisions.

Presley, M.A., Christensen, P.R., 1997. Thermal conductivity measurements of particulate materials: 1. A review. J. Geophys. Res. 102(E3), 6535–6549.

Putzig, N.E., Mellon, M.T., Kretke, K.A., Arvidson R.E., 2005. Global thermal inertia and surface properties of Mars from the MGS mapping mission. Icarus 173, 325–341, doi:10.1016/j.icarus.2004.08.017.

Rogers, A.D., Christensen, P.R., 2003. Age relationship of basaltic and andesitic surface compositions on Mars: Analysis of high-resolution TES observations of the Northern Hemisphere. J. Geophys. Res. 108, (E4), 5030, doi:10.1029/2002JE001913.

Rogers, A.D., Christensen, P.R., Bandfield, J.L. 2005. Compositional heterogeneity of the ancient Martian crust: Surface analysis of Ares Vallis bedrock with THEMIS and TES data, J. Geophys. Res. 110, E05010, doi:10.1029/2005JE002399.

Rogers, A.D., Christensen, P.R. 2007, Surface mineralogy of Martian low-albedo regions from MGS-TES data: Implications for upper crustal evolution and surface alteration, J. Geophys. Res., doi:10.1029/2006JE002727.

Rubin, A.E., Warren, P.H., Greenwood, J.P., Verish, R.S., Leshin, L.A., Hervig, R.L., Clayton, R.N., Mayeda, T.K., 2000. Los Angeles: The most differentiated basaltic Martian meteorite. Geology 28, 1011-1014.

Ruff, S.W., Christensen, P.R, Blaney, D.L., Farrand, W.H., Johnson, J.R., Michalski, J.R., Moersch, J.E., Wright, S.P., Squyres, S.W. 2006. The rocks of Gusev Crater as viewed by the Mini-TES instrument. J. Geophys. Res. 111, E12S18, doi:10.1029/2006JE002747.

Scott, D.H., Tanaka, K.L., 1986. Geologic map of the western equatorial region of Mars, scale 1:15,000,000. USGS Misc. Inv. Series map I-1802-A.

Shirley, D.N., 1987. Differentiation and compaction in the Palisades Sill, New Jersey. J. Petrol. 28-5, 835-865.

Squyres, S.W., and 18 colleagues, 2004a. In Situ Evidence for an Ancient Aqueous Environment at Meridiani Planum, Mars. Science 306, 1709-1714.

Squyres, S.W., and 49 colleagues, 2004b. The Spirit Rover's Athena Science Investigation at Gusev Crater, Mars. Science 305, 794-800.

Stolper, E., McSween, H.Y., Jr., 1979. Petrology and origin of the shergottite meteorites. Geochimica et Cosmochimica Acta 43, 1475-1498.

Streckeisen, A., 1976. To each plutonic rock its proper name. Earth Sci. Rev. 12, 1-33.

Taylor, L.A., et al., 2002. Martian meteorite Dhofar 9: A new shergottite. Meteorit. Planet. Sci. 37, 1107-1128.

Taylor, G. J., et al., 2006. Bulk composition and early differentiation of Mars. J. Geophys. Res. 111(E03S10), doi:10.1029/2005JE002645.

Treiman, A.H., McKay, G.A., Bogard, D.D., Mittlefehldt, D.W., Wang, M.-S., Keller, L., Lipschutz, M.E., Lindstrom, M.M., Garrison, D., 1994. Comparison of the LEW88516 and ALHA77005 martian meteorites: Similar but distinct. Meteoritics 29, 581-592.

Vincendon, M., Langevin, Y., Poulet, F., Pommerol, A., Wolf, M., Bibring, J.-P., Gondet, B., Jouglet, D., 2008. Yearly and seasonal variations of low albedo terrains on Mars in the OMEGA/Mex dataset: constraints on aerosols properties and dust deposits. Submitted to Icarus.

Wager, L.R., Brown, G.M., 1968. Layered Igneous Intrusions. Oliver & Boyd, Edinburgh & London, 588 pp.

Warren, P.H., Greenwood, J.P., Rubin, A.E., 2004. Los Angeles: A tale of two stones. Meteoritics & Planet. Sci. 39, 137-156.

Wyatt, M.B., McSween, H.Y., 2002. Spectral evidence for weathered basalt as an alternative to andesite in the northern lowlands of Mars. Nature 417, 263-266.

Zipfel, J., Scherer, P., Spettel, B., Dreibus, G., Schultz, L., 2000. Petrology and chemistry of the new shergottite Dar al Gani 476. Meteoritics & Planetary Science 35, 95-106.

Tables

Table 1. Properties of the studied terrains. Ages: E=Early, L=Late, M=Middle, N=Noachian, H=Hesperian, A=Amazonian. Acronyms of the study regions are indicated in parenthesis.

Name	Bounding coordinates	Age	Geomorphology
Meridiani (M)	358-3.5E, 1.5-6N	EN-LN	Sand predominant
Hesperia Planum (HP)	108-111E, 24-29S	EH	Sand predominant
Mare Siremun (MS)	207.5-209.5E, 34-37S	EH	Sand and rocks
Tyrrhena Terra (TT)	89-93E, 11-13S	LN-EH	Sand, rocks and bedrock
Protei Planum (PP)	308.0-308.5E, 21-29S	EH	Sand, rocks and bedrock
Solis Lacus (SL)	261.5-265E, 23.5-26.5S	LH	Bedrock predominant
Syrtis Major:			
- *Lavas (SML)*	65-69E, 1.5-12N	EH-LH	Sand predominant
- *Nili Patera (SMN1)*	67.51E, 8.77N	LH	Bedrock predominant
- *Nili Patera (SMN2)*	67.57E, 7.19N	LH	Sand dunes
Nili Fossae:			
- *Highlands (NFH)*	72.8-73.75E, 20.1-20.7N	EN-MN	Bedrock predominant
- *Olivine-rich terrains (NFO)*	76.84E, 23.23N	LN	Sand dunes
LCP-rich terrains in southern hemisphere (LCP):			
	101.25E, 24.12S	EN-MN	Outcrop (LCP1)
	309.42E, 35.95S	EN-MN	Outcrop (LCP2)
	302.54E, 15.43S	MN-LN	Outcrop (LCP3)
Young terrains:			
- *Echus Chasma floor(EC)*	280.25-280.75E, 0.75-0.5S	LA	Bedrock predominant
- *Noctis Labyrinthus (NL)*	263.7-264.5E, 7.0-7.5S	LA	Bedrock predominant

Table 2. OMEGA derived modal mineralogy (values in bold) for the large geographic areas and compared to the TES modal mineralogy (Rogers and Christensen, 2007). Values are percent and standard errors for OMEGA abundances indicate +/-1σ. Olivine is forsterite with particle size fixed at 100 μm.

	HCP	LCP	LCP/(HCP+LCP)	Neutral	Olivine	Others	RMS
				Components			
Syrtis Major lavas (SML)	**34+/-7**	**9+/-3**	**0.20+/-0.05**	**48+/9**	**<5**	**8+/-5**	**0.21+/-0.06**
	30+/-1	4+/-2	0.12+/-0.05	46+/6	7+/-1	13	
Tyrrhena Terra (TT)	**22+/-3**	**11+/-3**	**0.33+/-0.06**	**50+/-5**	**9+/-4**	**8+/-4**	**0.13+/-0.03**
	20+/-4	14+/-5	0.40+/-0.08	40+/-8	12+/-1	13	
Terra Meridiani (M)	**29+/-4**	**11+/-4**	**0.26+/-0.08**	**49+/-7**	**<5**	**7+/-4**	**0.25+/-0.03**
	22+/-2	3	0.12+/-0.01	49+/-6	7+/-1	14	
Mare Sirenum (MS)	**23+/-4**	**8+/-2**	**0.26+/-0.05**	**49+/-6**	**<5**	**15+/-5**	**0.22+/-0.03**
	20+/-1	7+/-2	0.25+/-0.05	56+/-6	5	12	
Hesperia Planum (HP)	**26+/-5**	**8+/-3**	**0.22+/-0.06**	**50+/-8**	**<5**	**12+/-8**	**0.23+/-0.03**
	20+/-1	10+/-4	0.30+/-0.08	43+/-3	11+/-1	14	
Solis Lacus (SL)	**23+/-5**	**7+/-3**	**0.23+/-0.08**	**47+/-10**	**< 5**	**15+/-10**	**0.25+/-0.03**
	6+/-2	15+/-4	0.70+/-0.20	62+/-10	6+/-1	9+/-1	
Protei Planum (PP)	**25+/-8**	**8+/-4**	**0.24+/-0.08**	**57+/-4**	**<5**	**7+/-5**	**0.21+/-0.03**
Echus Chasma (EC)	**25+/-6**	**6+/-3**	**0.19+/-0.09**	**47+/-10**	**< 5**	**17+/-13**	**0.26+/-0.03**
Noctis Labyrinthus (NL)	**30+/-5**	**8+/-3**	**0.20+/-0.07**	**48+/-7**	**< 5**	**12+/-9**	**0.39+/-0.04**

Table 3. Derived modal mineralogy for the Hesperian Syrtis lavas (see Table 2) compared to the average mineralogy of Noachian highlands in the region around the Nili Fossae and three LCP-rich outcrops of the southern hemisphere. Values are percent and standard errors for OMEGA abundances indicate +/-1σ.

	Syrtis Major Lavas (SML)	Nili Fossae highlands (NFH)	LCP-rich outcrops (LCP)
HCP	34+/7	26+/-3	30+/-7
LCP	9+/-3	11+/-3	20+/-5
LCP/(HCP+LCP)	0.20+/-0.05	0.30+/-0.06	0.40+/-0.10
Neutral Components	48+/-9	53+/-4	40+/-10
Olivine (100 μm)	<5	<5%	<5%
Others	8+/-5	6+/5	10+/-5

Table 4. Modeled phase abundances and particle size for olivine-bearing terrains.

	Nili Patera				Nili Fossae	
	SMN1		SMN2		NFO	
	Abundance (%)	Particle size (μm)	Abundance (%)	Particle size (μm)	Abundance (%)	Particle size (μm)
HCP	23	200	31	600	13	300
LCP	0	-	8	300	0	-
Plagioclase	57	20	30	800	48	20
Olivine	14	100	16	40	40	2500
Dust	6	5	15	5	0	-
RMS	0.27		0.14		0.21	

Table 5. Chemical composition (wt. %) and densities of each mineral used for the chemical calculation.

	Pigeonite	Diopside	Augite	Plagioclase	Forsterite	Magnetite
SiO_2	49.99	52.7	50,35	51.76	40.87	
TiO_2	0.53	0.34	0,36	0.00		0.00
Al_2O_3	6.21	1.84	2,21	30.84		0.21
FeO	16.56	5.42	16,18	0.00	9.77	30.78
Fe_2O_3	0.58	2.12	1,69	0.00		68.85
MnO	0.26	0.16	0,37	0.00		
MgO	22.31	15.15	11,15	0.00	49.36	0.00
CaO	3.99	21.58	17,93	13.36		
Na_2O	0.06	0.49	0,23	3.86		
K_2O	0.00	0.00	0,03	0.17		
Total	100.49	99.8	100.5	99.99	100.00	99.84
Density	3.3	3.3	3.3	2.7	3.4	5.2

Table 6. Calculated chemical compositions for the studied low albedo regions. The values are calculated for a 2 vol. % of iron oxide, a 2.5% of olivine (Fo 90) and in assuming a sum to 100.

	Syrtis Lavas	Tyrrhena	Meridiani	Protei	Mare Sirenum	Hesperia	N. Fossae highlands	LCP-rich outcrops	Solis Lacus	Echus Chasma	Noctis
SiO_2	49.8+/0.3	48.7+/-0.4	49.6+/-0.3	49.6+/-0.5	49.4+/-0.3	49.5+/-0.3	49.6+/-0.3	49.3+/-0.5	49.3+/-0.3	49.4+/-0.3	49.6+/-0.3
TiO_2	0.2	0.2	0.2	0.1	0.2	0.2	0.2	0.2	0.2	0.2	0.2
Al_2O_3	15.1+/-2.2	15.9+/-0.7	16.0+/-1.5	18.1+/-2.0	17.3+/-1.9	16.9+/-1.9	16.9+/-0.9	14.8+/-3.4	17.0+/-2.4	16.9+/-2.6	15.9+/-1.7
FeO	5.2+/-0.7	5.7+/-0.5	5.4+/-0.8	4.5+/-0.7	4.9+/-0.7	4.9+/-0.7	5.2+/-0.5	6.4+/-1.1	5.1+/-0.9	4.8+/-0.9	5.0+/-0.6
Fe_2O_3	3.3+/-0.2	3.1+/-0.1	3.3+/-0.1	3.2	3.5+/-0.2	3.4+/-0.2	3.2+/-0.1	3.5+/-0.1	3.6+/-0.3	3.6+/-0.3	3.4+/-0.2
MnO	0.1	0.1	0.1	0.1	0.1	0.1	0.1	0.1	0.1	0.1	0.1
MgO	9.6+/-0.5	12.0+/-0.7	9.4+/-0.3	8.0+/-0.4	8.5+/-0.2	8.7+/-0.3	8.9+/-0.2	10.7+/-1.2	8.7+/-0.6	8.5+/-0.6	9.2+/-0.2
CaO	14.7+/-0.7	12.3+/-0.5	14.0+/-0.3	14.0+/-0.7	13.9+/-0.6	14.1+/-0.6	13.8+/-0.4	13.2+/-0.9	13.9+/-0.6	14.3+/-0.8	14.5+/-0.6
Na_2O	1.9+/0.3	2.0+/-0.1	2.0+/-0.2	2.3+/-0.3	2.2+/-0.2	2.1+/-0.3	2.1+/-0.1	1.8+/-0.4	2.1+/-0.3	2.1+/-0.3	2.0+/-0.2
K_2O	0.1	0.1	0.1	0.1	0.1	0.1	0.1	0.1	0.1	0.1	0.1
Total	100.0	100.0	100.0	100.0	100.0	100.0	100.0	100.0	100.0	100.0	100

Captions:

Fig. 1. Names and locations of extended geographic areas discussed in this work. The background image is the map of the pyroxene spectral parameter ranged between 0.01 and 0.06 (Poulet et al., 2007). The red stars indicate the locations of the studied young terrains.

Fig. 2. Olivine map over the Major Syrtis and Nili Fossae regions (adapted from Poulet et al. 2007). Eroded terrains (referred as to SMN1 in Table 1) and dunes (SMN2) in Nili Patera region (central caldera of Syrtis Major) respectively identified by THEMIS images and MOC image will be examined. The mineralogy of one spot in Nili Fossae (NFO) identified by the white circle on the olivine map is also studied.

Fig. 3. Context images of some of the Noachian age areas. (a) Nili Fossae highlands surrounded by Syrtis Major volcanic flows (HRSC image 1347 centered at 73.2°E, 20.4°N). (b) Highland outcrop number 1 surrounded by lava plains (THEMIS mosaic centered at 101.2°E, 24.1°S). (c) Highland outcrop number 3 corresponds to the central hills of this canyon, which is part of the lower flanks of Valles Marineris walls (THEMIS mosaic centered at 302.5°E, 15.4°S).

Fig. 4. Context images of the areas selected in Hesperian volcanic plains from daytime THEMIS mosaic (a, c, d, f) and night time THEMIS mosaic (b, e). (a) Solis Planum (b) Tyrrhena Terra (c) Protei (d) Hesperia (e) Mare Sirenum (f) Syrtis. Images show homogeneous terrain for Syrtis, Hesperia and Protei.

Fig. 5. Context images of the areas selected in Amazonian regions. (a) HRSC image 1977 inside Noctis Labyrinthus, centered on coordinates 263.7°E, 7.5°S. . This image shows a flat area of low albedo enriched in pyroxenes. (b) HRSC image 71 showing platy shaped patterns on a flat surface inside Echus Chasma floor. The image is entered on coordinates, 280.5°E, 0.5°S. Low albedo, pyroxenes signatures and platy patterns suggest volcanic flows filled this canyon.

Fig. 6. Spectra extracted from different low albedo regions compared to their best fit model in red. Each spectrum corresponds to one OMEGA pixel. Left, from top to bottom: Syrtis Major lavas (SML), Hesperia Planum (HP), Nili Fossae olivine-rich terrain (NFO), Echus Chasma (EC), Terra Tyrrhena (TT). Right, from top to bottom: Hesperia Planum (HP), LCP-rich outcrop (LCP1), olivine-rich dunes in Nili Patera (SMN2), Solis Planum (SL), Terra Tyrrhena (TT). For TT and HP, two spectra are shown to emphasize the spectral diversity of these regions. The RMS values are in the 0.11-0.28% range depending on the spectrum.

Fig. 7. RMS value versus the lambertian albedo at 1.08 μm for the analyzed OMEGA pixels extracted from the Syrtis Major region.

Fig. 8. Average particle size of plagioclase, HCP and LCP for the regions listed in Table 2.

Fig. 9. Compositional distribution of studied regions projected onto the ternary diagram with pyroxenes (HCP+LCP), olivine and plagioclase as vertices. The Amazonian terrains are represented by blue triangles. For the olivine-free regions, the olivine abundance that is found to be lower than 5%, is fixed to 2.5%. Gusev soil and rocks (black triangles) are plotted (McSween et al. 2006b; 2008). Acronyms of the regions are defined in Table 1.

Fig. 10. Same as Fig. 9 but with the LCP, Olivine, HCP vertices.

Fig. 11. FeO* / MgO vs. SiO_2 diagram. FeO* is the total Fe as Fe^{2+}. TH (tholeiitic) and SA (sub alkaline) fields are represented. Green triangle: OMEGA data (Table 6) calculated for 2 wt. % of iron oxides. The dotted lozenge area corresponds to uncertainties due to iron oxide variations of 2 ± 1 vol. %. The black cross indicates the error bar due to the uncertainties on the OMEGA-derived modal abundances. TES 1 and TES 2 fields: TES-derived compositions. Black stars: APXS analysis from Gusev crater (McSween et al., 2008); blue dot: basaltic Shergottites compiled by McSween et al. (2003); yellow squares: early proterozoic ferro-picrites from Baltic Shield, Kola Peninsula (Hanski and Smolkin, 1989).

Fig. 12. Same as Fig. 9 but with the mineralogy of different Shergottites (blue squares for basaltic Shergottites, green squares for picritic Shergottites, namely Dhofar019, EETA79001, SAU005/094, DAG476/489, NWA1068/1100, and black star for ALH). The modal mineralogy of the Martian meteorites comes from various sources: McSween et al. (1996); Hamilton et al. (2003); Warren et al. (2004); Ikeda et al. (2006); Meyer (2008).

Fig. 13. Same as Fig. 10 but with the mineralogy of different SNCs (blue squares for basaltic Shergottites and black stars for other SNCs). The modal mineralogy of the SNCs comes from various sources: Treiman et al. (2004); McSween et al. (1996); Hamilton et al. (2003); Warren et al. (2004); Ikeda et al. (2006); Meyer (2008).

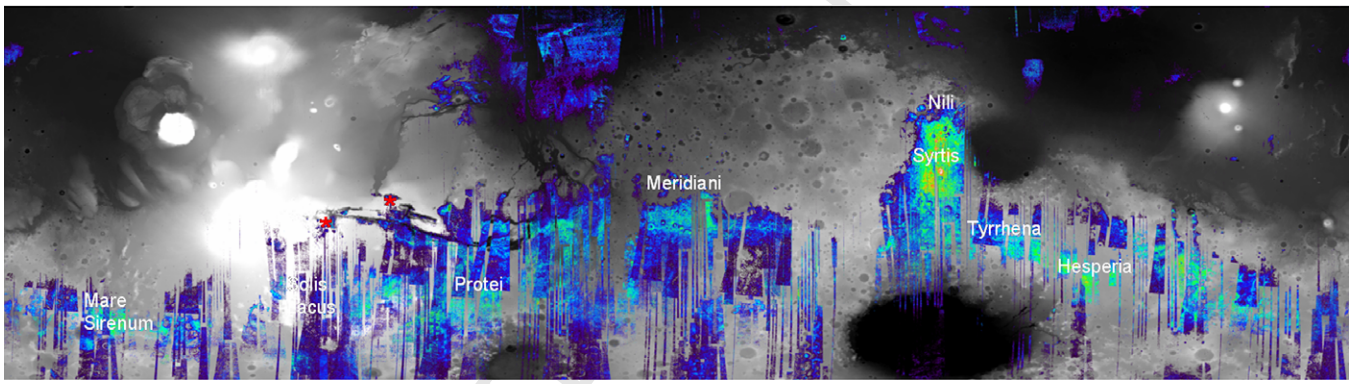

I10571_Fig1

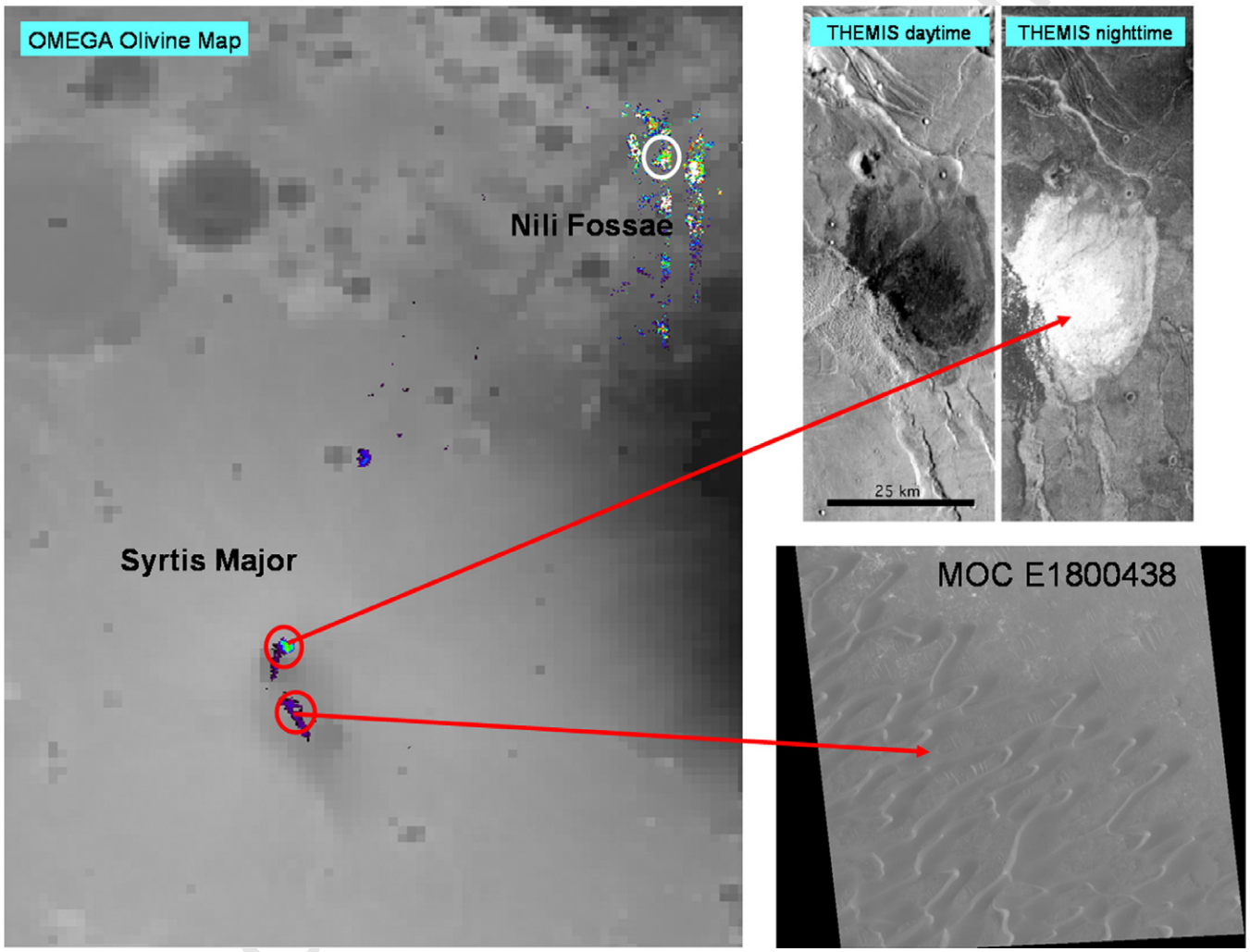

I10571_Fig2

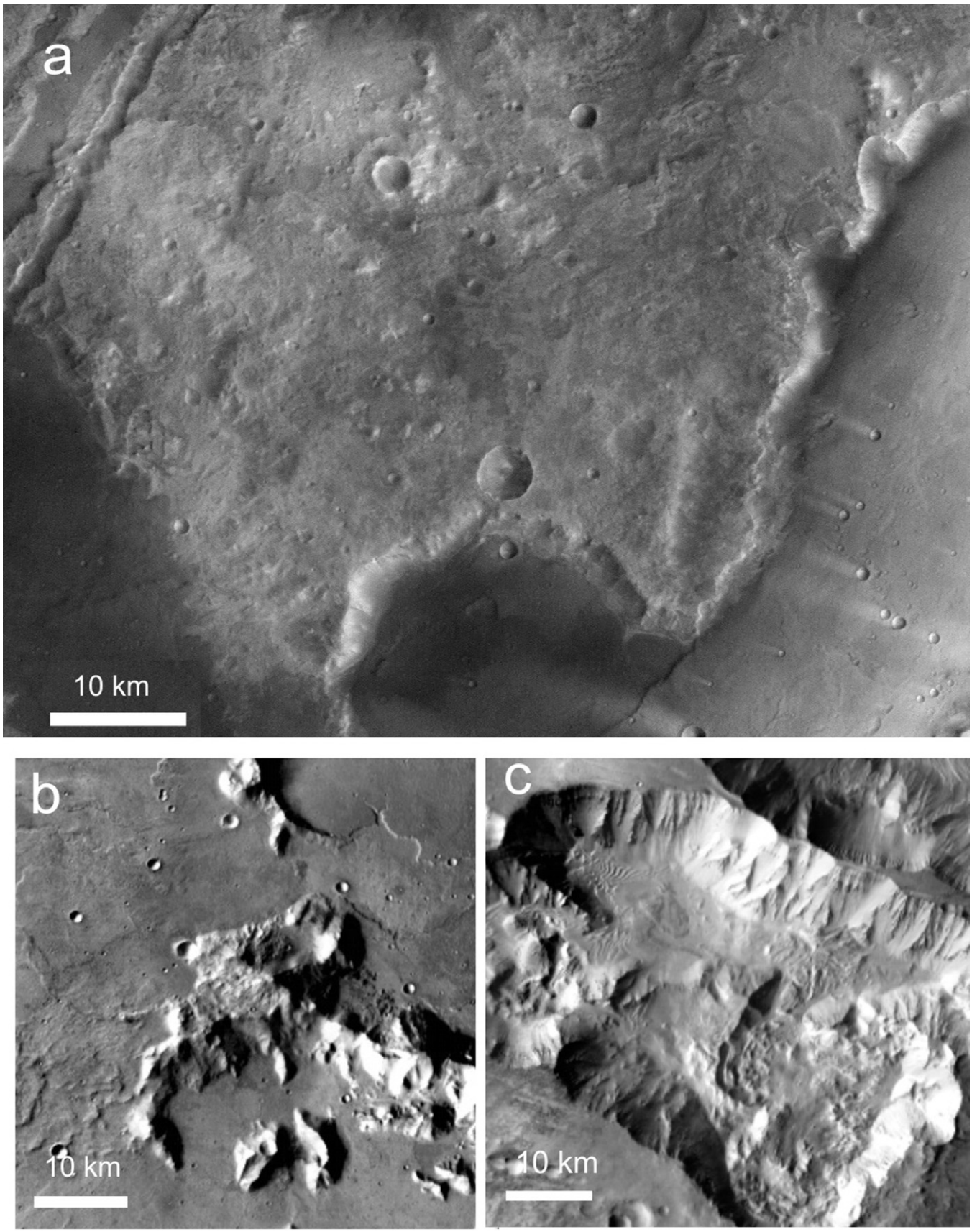

I10571_Fig3

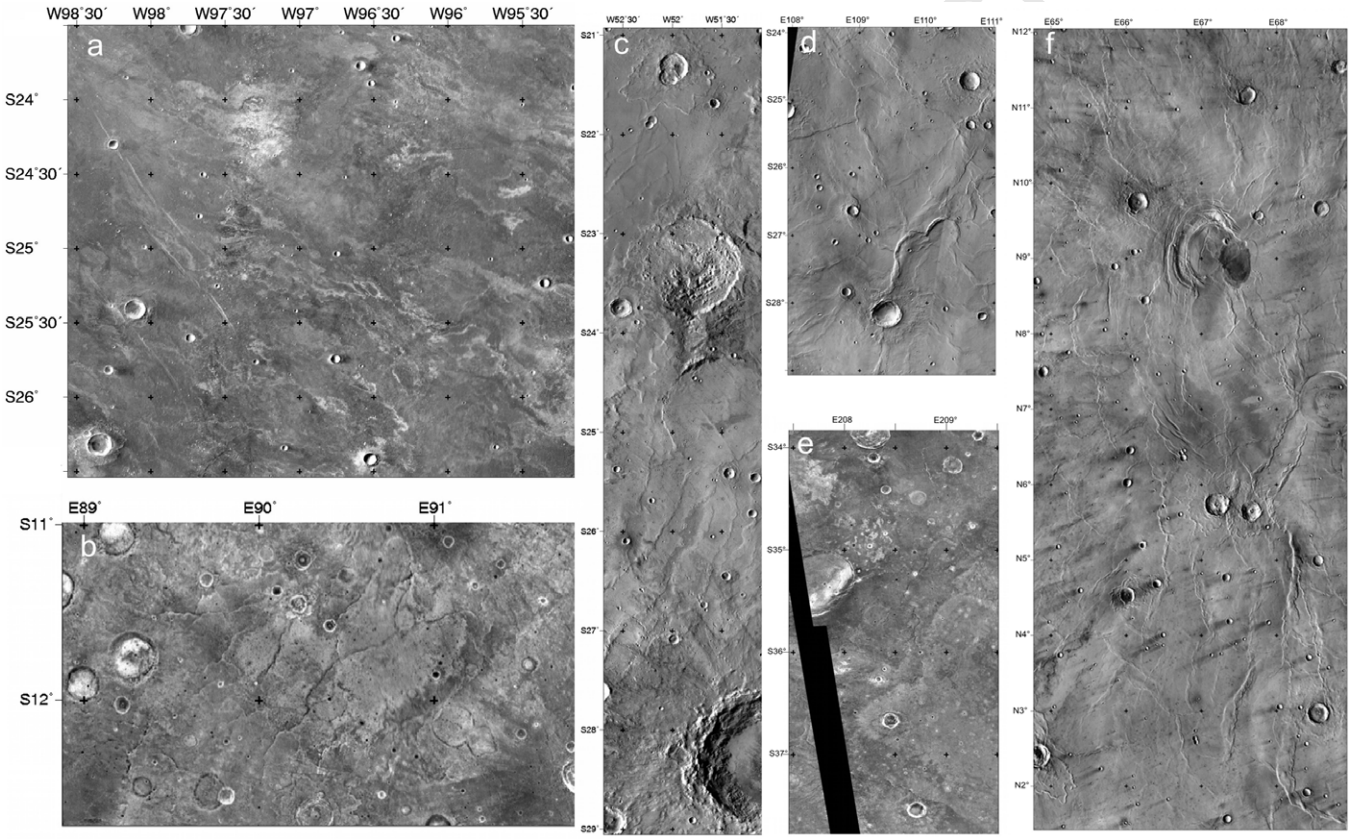

I10571_Fig4

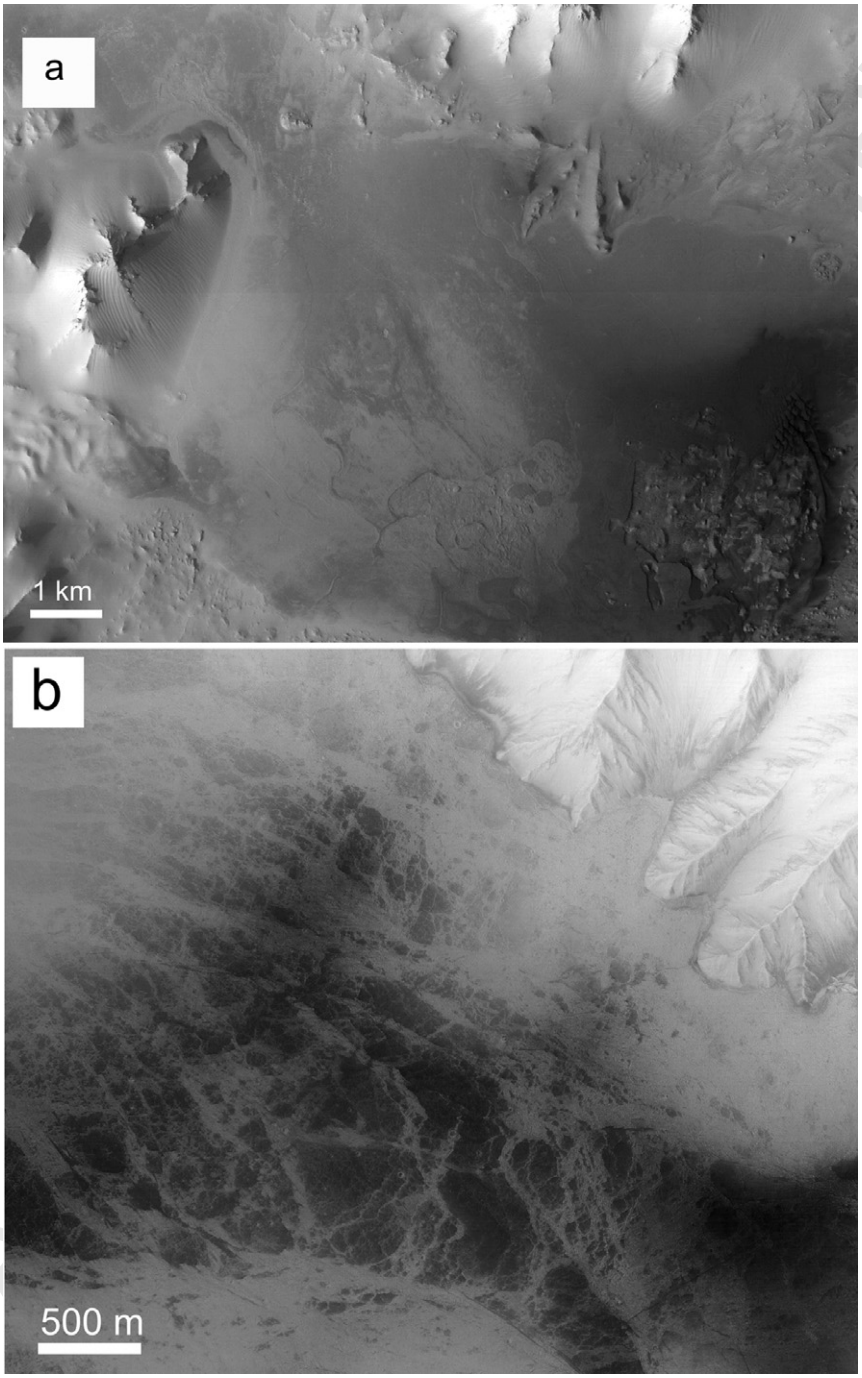

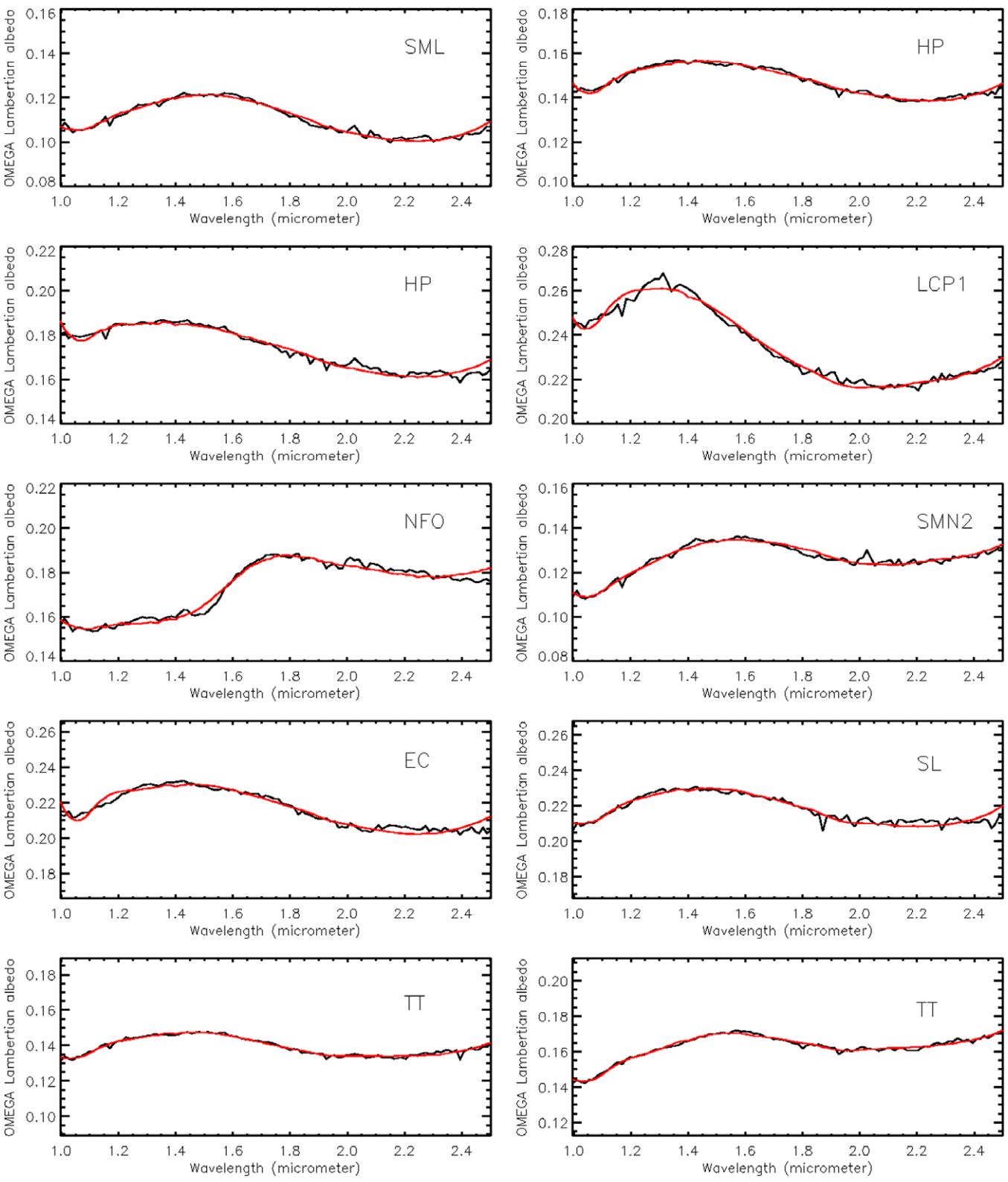

I10571_Fig6

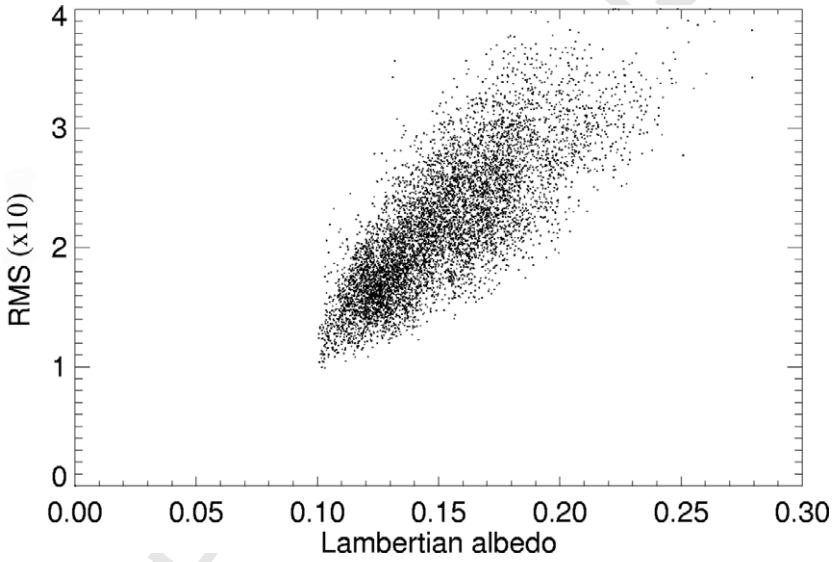

I10571_Fig7

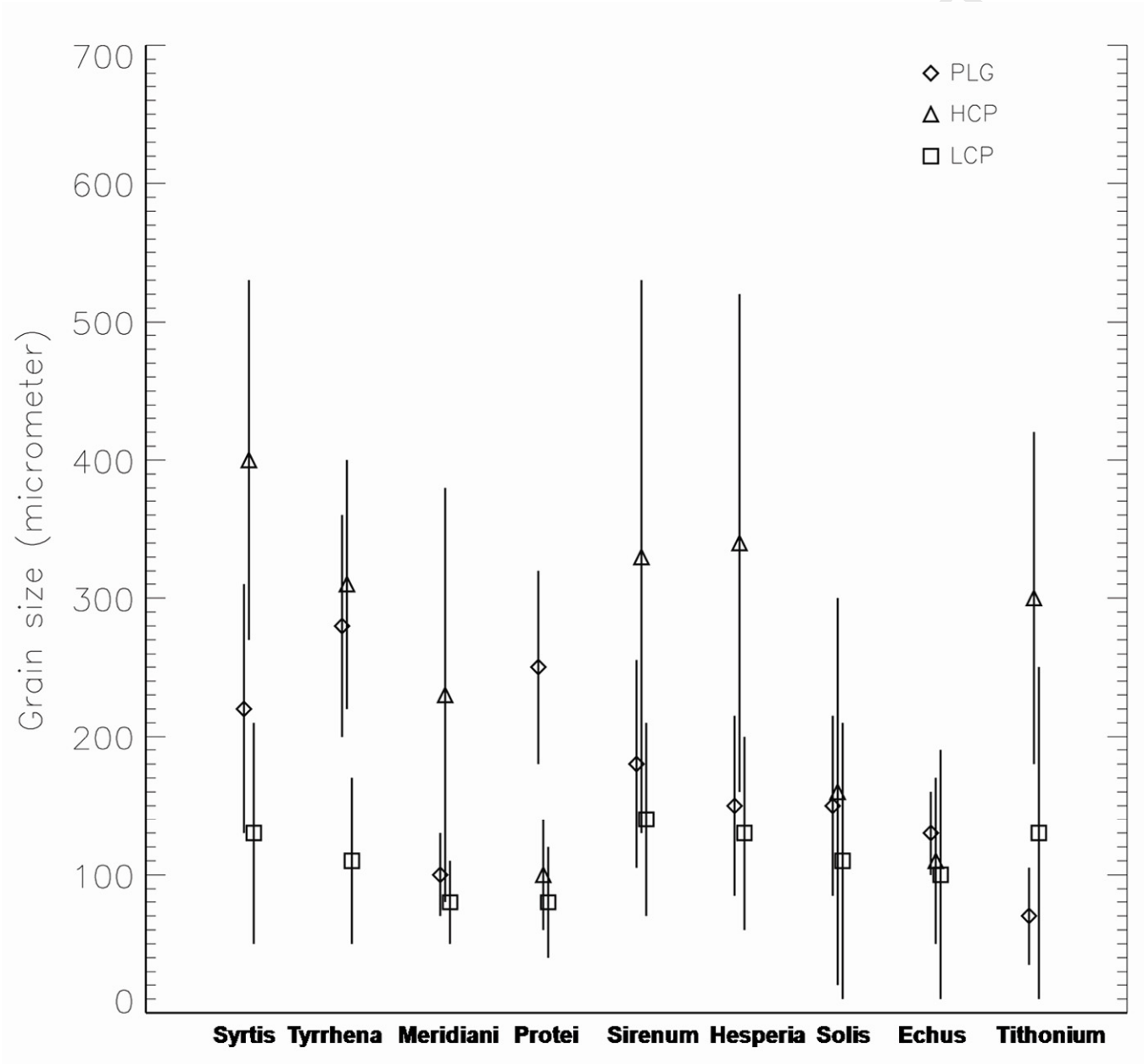

I10571_Fig8

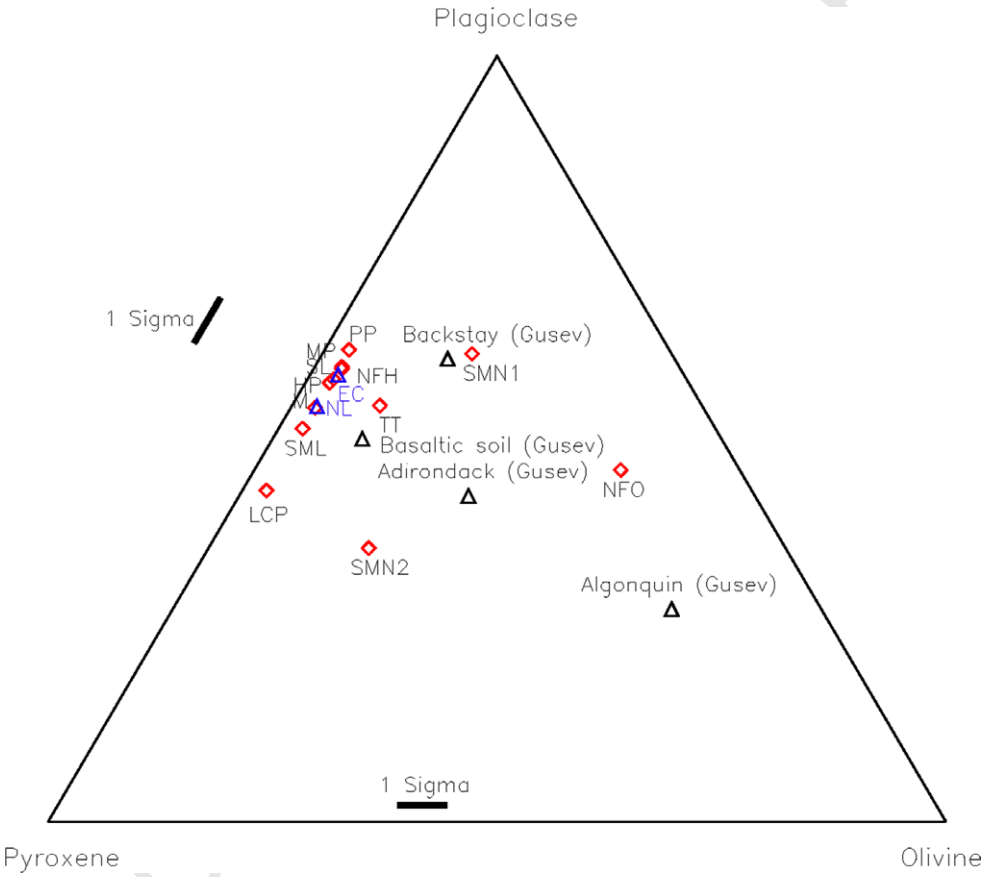

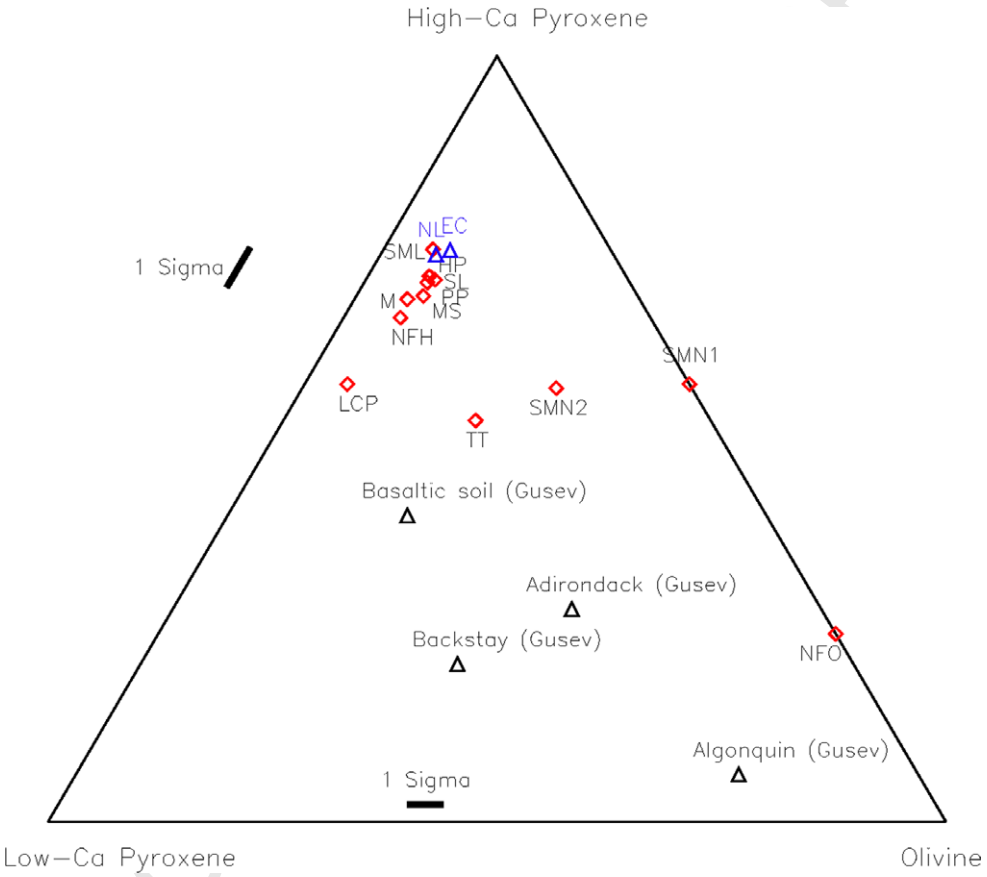

I10571_Fig10

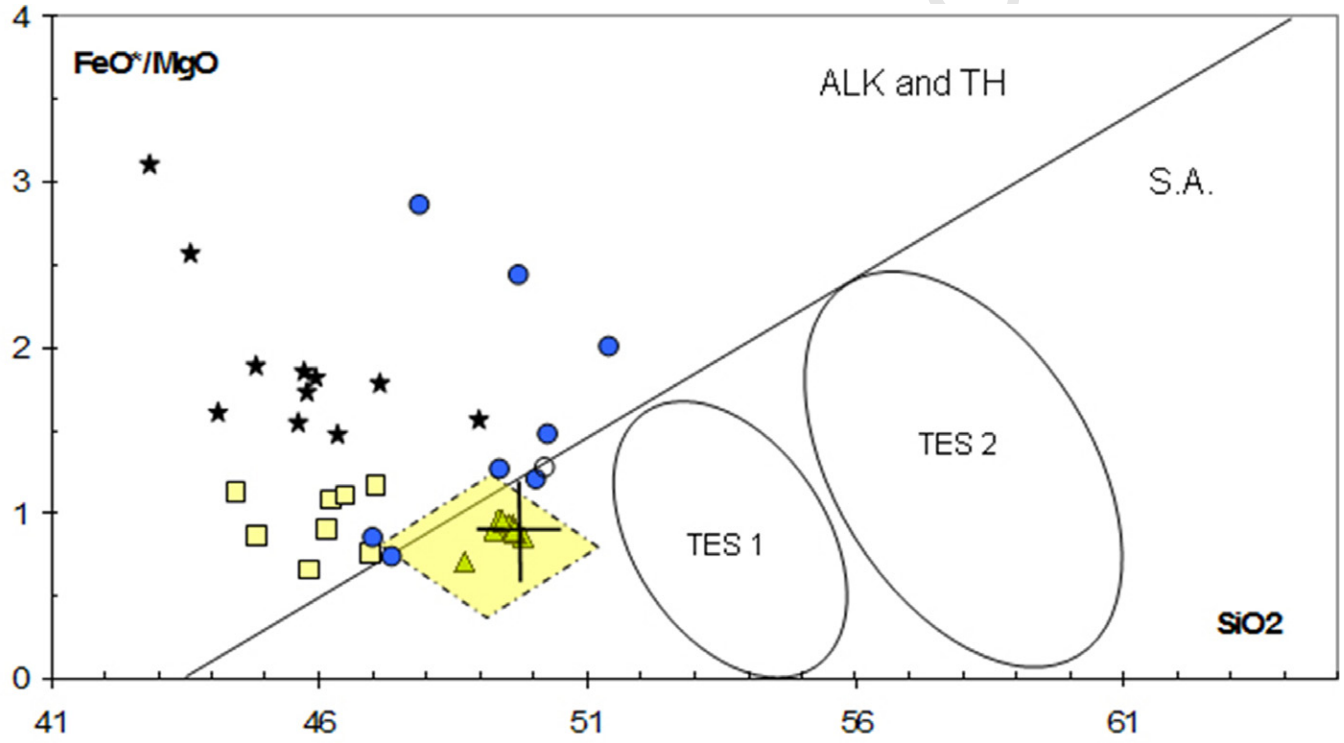

I10571_Fig11

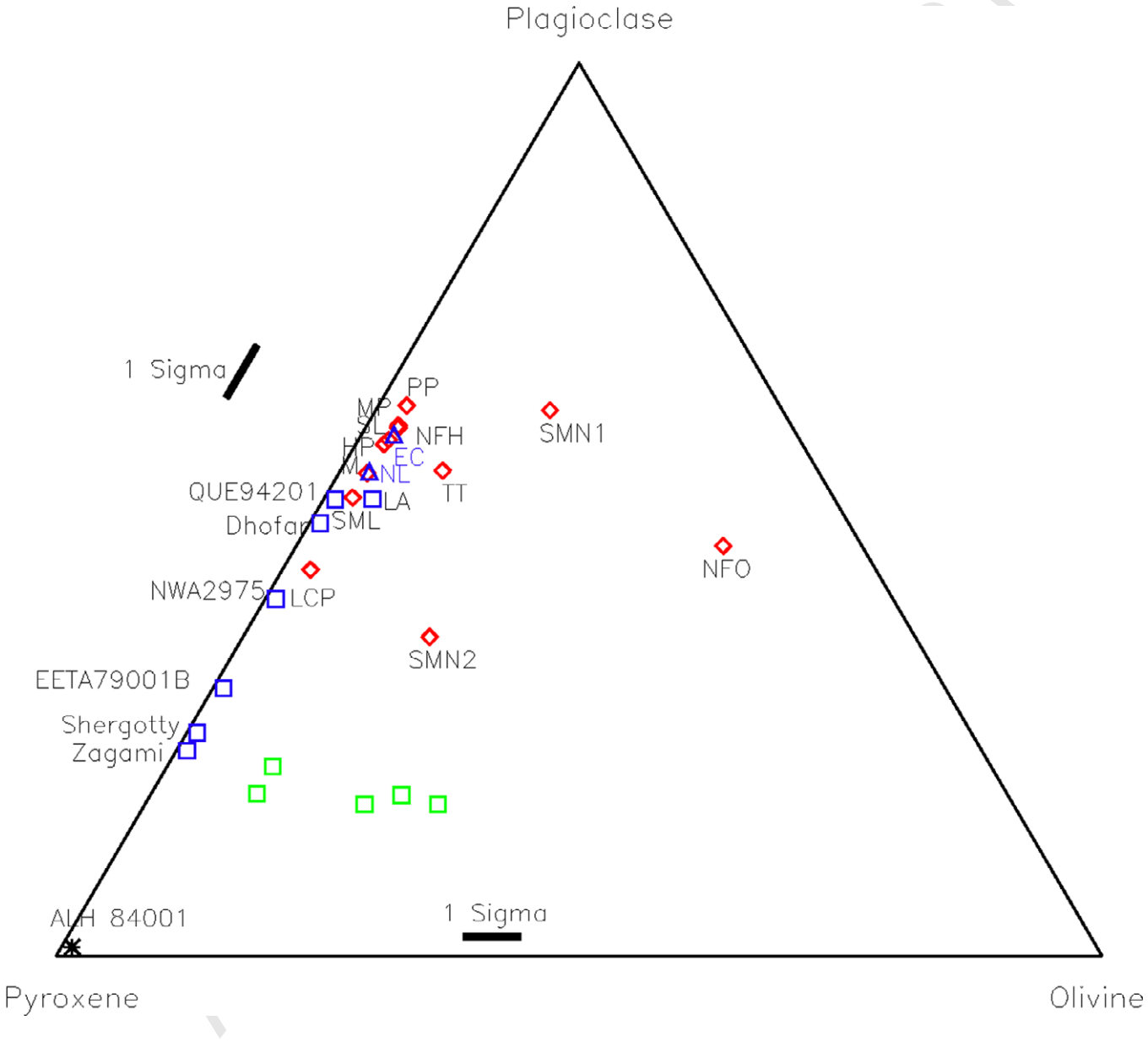

I10571_Fig12

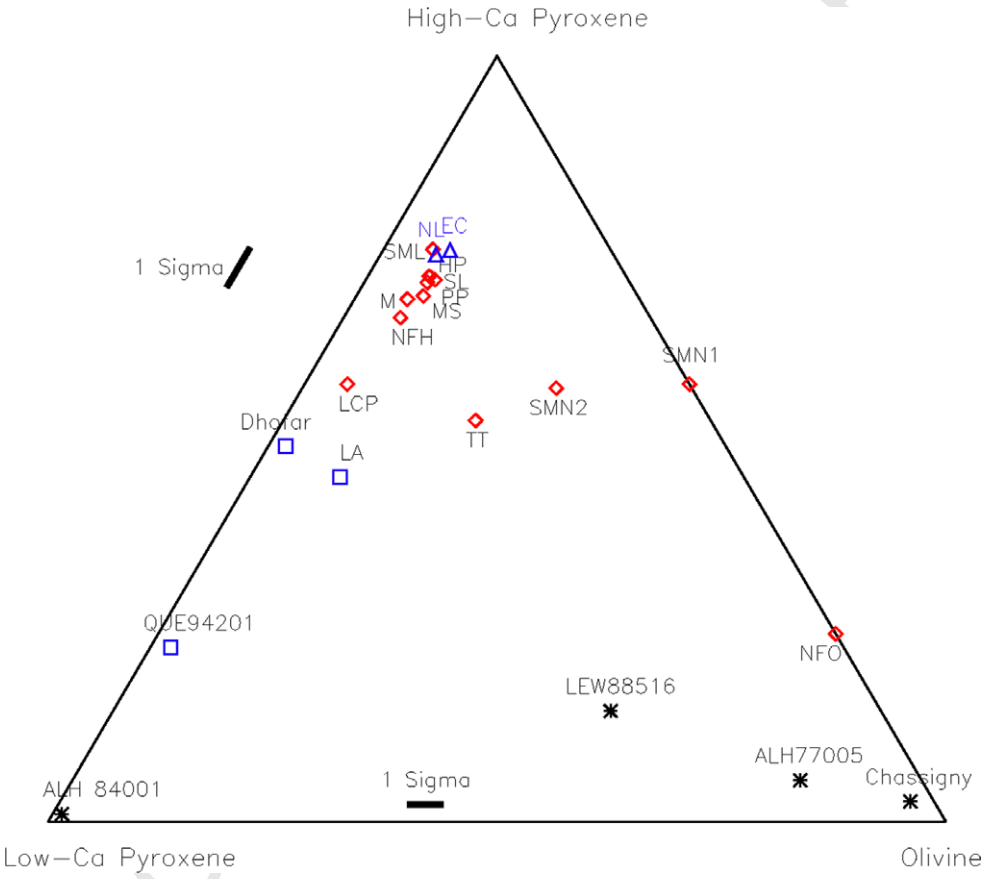

I10571_Fig13